Modeling Microglia Activation in Neuroinflammation in 3D Neural Spheroids After Single and Repeated Mild Traumatic Brain Injury

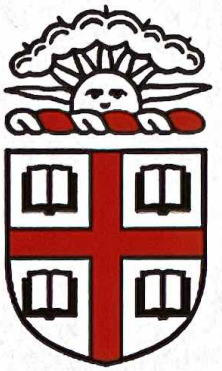

BROWN

Authored By

Lisa Okazaki

Master of Science, Brown School Of Engineering

Thesis

Submitted in partial fulfillment of the requirements for the Degree of Master of Science in the Graduate Program of Biomedical Engineering at Brown University

PROVIDENCE, RHODE ISLAND

MAY 2022

AUTHORIZATION TO LEND AND REPRODUCE THE THESIS

As the sole author of this thesis, I authorize Brown University to lend it to other institutions for the purpose of scholarly research.

Date 4/21/22 Lisa Okazaki

YOUR NAME, Author

I further authorize Brown University to reproduce this thesis by photocopying or other means, in total or in part, at the request of other institutions or individuals for the purpose of scholarly research.

Date 4/21/22 Lisa Okazaki

YOUR NAME, Author

This thesis by Lisa Okazaki is accepted in its present form by the Center for Biomedical Engineering as satisfying the thesis requirements for the degree of Master of Science

Date 4/21/2022 Signature: _____

Dr. Diane Hoffman-Kim, Advisor

Date 04/21/2022 Signature: _____

Dr. Haneesh Kesari, Reader

Date 4/21/22 Signature: _____

Dr. Judy Liu, Reader

Approved by the Graduate Council

Date _____ Signature: _____

Dr. Andrew G. Campbell, Dean of the Graduate School

Table of Contents

Acknowledgements **6**

Abstract **7**

Introduction **8**

TBI Diagnosis 8

Types of TBI Injuries 10

Neuroinflammation 11

Models of TBI 15

Mode of Injury 16

Research Aims 17

Methods **18**

Cell Isolation and Culture 18

3D Cortical Spheroid Culture 19

2D Antibody Dilution 19

Centrifugation Injury 20

LPS and Rosiglitazone Exposure 21

Immunohistochemistry 22

Imaging 24

ImageJ Analysis 24

Calculations for Total Mean Pixel Intensity and Sphericity 29

Statistics and Graphs 32

Results **32**

2D Dilution Testing for CD86 32

3D Experiments for CD86 and CD16 34

2D Antibody Dilutions for Iba-1, P2Y12R, CD206 38

Mean Pixel Intensities for CD206 40

Mean Pixel Intensities and Sphericity Measurements for P2Y12R 47

Discussion **56**

CD86 and CD16 Expression 58

P2Y12R Expression 60

CD206 Expression 62

Limitations 64

Future Directions 65

Conclusion **66**

References **67**

Acknowledgements

I would like to thank Dr. Diane Hoffman-Kim for giving me the opportunity to continue my research with her in the lab for my Master's program. She has continued to support me in both my research and academic career, and has served as a valuable mentor these past few years. She has helped push me to become the best researcher that I can be.

Next, I would like to thank Dr. Rafael D. Gonzalez-Cruz for his mentorship and insight for this TBI project. From looking at live/dead assays in my undergraduate thesis to looking at neuroinflammatory models in my Master's thesis, Dr. Gonzalez-Cruz has tremendously supported my work. I am incredibly grateful for the time that he spent helping me on this project.

I would also like to thank the rest of the Hoffman-Kim laboratory for their continued support these past few years. Everyone in the lab is always ready to help, and is ready to give me insightful feedback to help me become a better researcher. I would like to particularly thank Liane Livi for her instruction on how to appropriately handle the biomarkers, as well as conduct immunostaining. I would also like to thank Ahbid Zein-Sabatto for his support on the statistical analysis conducted on this project.

Finally, I would like to thank my family and friends for supporting me throughout my academic career. I am endlessly grateful for their encouragement throughout these past few years.

Abstract

About 1.5 million people in the US sustain a Traumatic Brain Injury (TBI), with 80-90% of those being mild traumatic brain injuries (mTBIs). mTBIs are characterized by headaches, dizziness and impaired memory. TBI is followed by cellular events such as excitotoxicity, free radical creation, and neuroinflammation in the brain. Neuroinflammation in particular is one of the most common and important consequences of TBI. Microglia play a key role in neuroinflammation, as they are the primary immune effector cells within the CNS microenvironment. Following injury, microglia changes from resting-state to an activated state, resulting in a change in morphology. The activated state falls on an activation spectrum between two major phenotypes, commonly classified as M1 or M2, which describe its pro-inflammatory and anti-inflammatory states respectively. This study employs a three-dimensional (3D) neural spheroid model that was developed by the Hoffman-Kim laboratory, that mimics the brain microenvironment. Centrifugal injuries at 4,000 revolutions per minute (RPM) were applied to the spheroids to mimic the mTBI, with either single injury or three consecutive injuries for repeated conditions. These spheroids were then fixed at various time points ranging from immediately after injury at 0H to 7 DPI (days post injury). These spheroids were then stained for CD86 and CD16 as M1 markers, and CD206 as an M2 marker. In order to determine the microglia's resting state, the P2Y12 receptor is used, as it is a microglia-specific marker that is highly expressed in the resting state of microglia. In this study, the total mean pixel intensities and sphericities for the spheroids were calculated using ImageJ, and it found that there was a significant difference in total mean pixel intensities and sphericities for three repeated injury conditions stained for P2Y12R. Significant differences were found in total mean pixel intensities and sphericities between 0H and 7DPI in repeated conditions for CD206, but there were no other significant differences found in the rest of the CD206 conditions tested. CD86 and CD16 were not detected at any of the tested conditions. This study establishes a 3D spheroid model to study neuroinflammatory markers for microglia in both single and repeated mTBI injuries, particularly looking at mean pixel intensities of the stainings as well as the morphology.

Introduction

Traumatic Brain Injury (TBI) is defined as an injury that disrupts brain function, caused by a sudden and violent collision to the head by another object, or when an object penetrates the skull and brain tissue (*Traumatic Brain Injury – Causes, Symptoms and Treatments*, n.d.; *Traumatic Brain Injury Information Page*, n.d.).

Annually, about 70 million people suffer from TBI every year, in which 1.5 million of those cases are experienced in the US (Pankratova et al., 2021; *Report to Congress*, 2019). In 2014, there were about 2.87 million cases of TBI that occurred in the United States, with a reported 288,000 hospitalizations every year (*Traumatic Brain Injury – Causes, Symptoms and Treatments*, n.d.). With 50,000 deaths annually, TBI accounts for about 30.5% of all injury-related deaths (*Traumatic Brain Injury – Causes, Symptoms and Treatments*, n.d.; Younger et al., 2019). The high prevalence of TBI created a substantial financial burden. The global economic burden is estimated to be about 400 billion dollars, indicating that 1 out of every 200 dollars created in the global economy is spent to pay for the costs of TBI (Pankratova et al., 2021).

TBI Diagnosis

TBI is typically diagnosed based on medical history, neurological examination, neuroimaging tools, and clinical assessment scales. Neuroimaging tools encompass computed tomography (CT), magnetic resonance imaging (MRI), single-photon emission computed tomography (SPECT), and positron emission tomography (PET) (Pankratova et al., 2021). Although there are multiple clinical assessment scales, the Glasgow Coma Scale (GCS) is the most popular because it is simple and easy to use as a standardized assessment tool. It consists of a sum score of the eye, motor and verbal components. The scores demonstrate severity of injury in which a score of 13-15 represents mild TBI, a score of 9-12 represents moderate TBI, and a score of less than 8 represents severe TBI (Teasdale et al., 2014).

Mild traumatic brain injury (mTBI) is the most common form of brain injury, accounting for about 80-90% of TBI cases (Levin & Diaz-Arrastia, 2015). Some of the most common mTBI symptoms are headache, dizziness and impaired memory. Secondary injuries can cause the development of progressive degeneration, which can lead to enduring physical, cognitive and neuropsychological impacts including seizures, sleep disorders, depression, and blurry vision (Cole & Bailie, 2016; Lucke-Wold et al., 2018). While symptoms usually subside within 10 days of injury for most patients, 10-40% experience persistent symptoms known as post-concussion syndrome (PCS), and recent research has suggested that PCS is more common than previously thought (Fehily & Fitzgerald, 2017; McInnes et al., 2017).

Clinical research has shown that while a single mTBI may not have a significant impact on the brain, repeated injuries can create a cumulative effect both by increasing vulnerability for further mTBI and advancing progression to long-term functional deficits. Repeated mTBI is connected to increased severity in cognitive, behavioral and motor complications that can last for years (Kulkarni et al., 2019). For example, in retired American football players, it has been demonstrated that repeated mTBI has resulted in increased rates of cognitive impairment, increased susceptibility to chronic traumatic encephalopathy (CTE), Alzheimer's disease, and psychiatric illness (Fehily & Fitzgerald, 2017; Guskiewicz et al., 2005).

A large portion of the US population is at risk for these repetitive mTBIs, particularly from participating in sports or military service. High frequencies of brain injuries have been reported in collision sports such as soccer, rugby, and American football, especially from collisions between players (Slemmer et al., 2002). Among military personnel, common causes of repetitive mTBI include blast exposure, and 42% of Afghanistan and Iraq veterans with history of mTBI reporting PTSD symptoms (Fehily & Fitzgerald, 2017; Kontos et al., 2013).

One of the greatest challenges with TBI is its difficulty in diagnosis. While TBI is typically diagnosed using GCS and neuroimaging techniques, both of these options fail to accurately diagnose mTBI, which represent the majority of cases (Di Pietro et al., 2017). There are multiple layers to this

issue, including the lack of interdisciplinary consensus regarding the diagnostic criteria and management of TBI (Prince & Bruhns, 2017). GCS has also been shown to be unreliable in differentiating between mild and moderate TBIs and produces a poor prediction of patient outcome (Pankratova et al., 2021). The reliance on the patient's subjective responses for diagnostic evaluation, also serves as a weakness in the diagnostic process. The symptoms of mTBI can be obscure, and some patients may ignore, mask, or exaggerate their symptoms (Jeter et al., 2013). Furthermore, conventional neuroimaging techniques like CT and MRI have proven to be ineffective at detecting subtle changes in the brain including diffuse axon injury (DAI), the most common injury in mTBI patients (Koerte et al., 2016). These neuroimaging techniques are also costly and not readily available onsite, especially in the battlefield or sports facilities (Pankratova et al., 2021).

Types of TBI injuries: primary vs secondary

The extent and severity of brain damage following TBI differs depending on the type, intensity, duration, and frequency of the impact (Maas et al., 2008). TBI damage to the neuronal tissues can be classified into primary and secondary injuries. Primary injury occurs directly after the primary external impact, and can result in microvascular injuries, axonal shearing, and cortical contusions (Najem et al., 2018). Primary injury is considered as the focal injury period, which can then potentially progress to secondary injury (Capizzi et al., 2020). Secondary injury, which can occur from minutes to days after the primary impact, develops from the complex biochemical cascade resulting from the cell membrane disruption.

There are two types of primary injury: focal and diffuse brain injuries. Depending on the presence of a focal lesion, primary injuries can be either focal, diffuse or both . Although both types of injuries are often present in TBI patients, diffuse axonal injury (DAI) accounts for about 70% of all TBI cases. Focal injuries can include subdural and epidural hematoma, and contusions, whereas DAI can include axonal injury, microvascular injury, and hypoxic-ischemic injury (Mckee & Daneshvar, 2015). Focal injuries are

characterized by concentrated neuronal and glial cells undergoing necrosis at the site of the contusion with decreased blood supply. Focal injuries can lead to behavioral impacts, cognitive deficits, and hemiplegia. On the other hand, DAI is caused by shearing and stretching of cerebral brain tissue due to rapid deceleration and acceleration forces. This damages neuronal axons, oligodendrocytes, and vasculature, which can then lead to brain edema and ischemic brain damage (Smith et al., 2003).

Secondary injury develops through a combination of several pathways including 1) excitotoxicity due to overproduction of neurotransmitter glutamate, 2) free radical creation which can cause damage to proteins and neural cell membranes, and 3) neuroinflammation involving both local and systemic activation of the immune system (Jassam et al., 2017). Other factors that contribute include mitochondrial dysfunction, liquid peroxidation, and apoptotic cell death (Ng & Lee, 2019). Unlike primary injuries, the progression of secondary injuries can be delayed using neuroprotective agents to prevent cell death (Najem et al., 2018).

Neuroinflammation

Neuroinflammation is one of the key aspects of secondary injuries in mTBI and is conceptualized as a double-edged sword, due to its beneficial and detrimental effects (McGinn & Povlishock, 2016). Post-traumatic neuroinflammation can be favorable because it involves the clearing of debris and promotes regeneration, but it can be also be detrimental by encouraging neuronal cell death and continued neurodegeneration. It is a complex reaction between central and peripheral cellular and soluble factors, that are influenced by age, sex, injury type, injury severity, secondary insults, and genetics (Simon et al., 2017). The inflammatory response is mediated by the activation of resident immune cells in the central nervous system (CNS) and from infiltration of peripheral immune cells due to the disruption of the blood brain barrier. This neuroinflammatory response results in the development of cerebral edema and increased intracranial pressure (McGinn & Povlishock, 2016).

The mechanical injury to the head causes primary tissue damage that induces neuroinflammation via the release of intracellular and intra-axonal components, extravasated blood factors, and increased free radical production and oxidative stress (McGinn & Povlishock, 2016). Local CNS microglia is also activated, proliferated, and recruited to the site of injury.

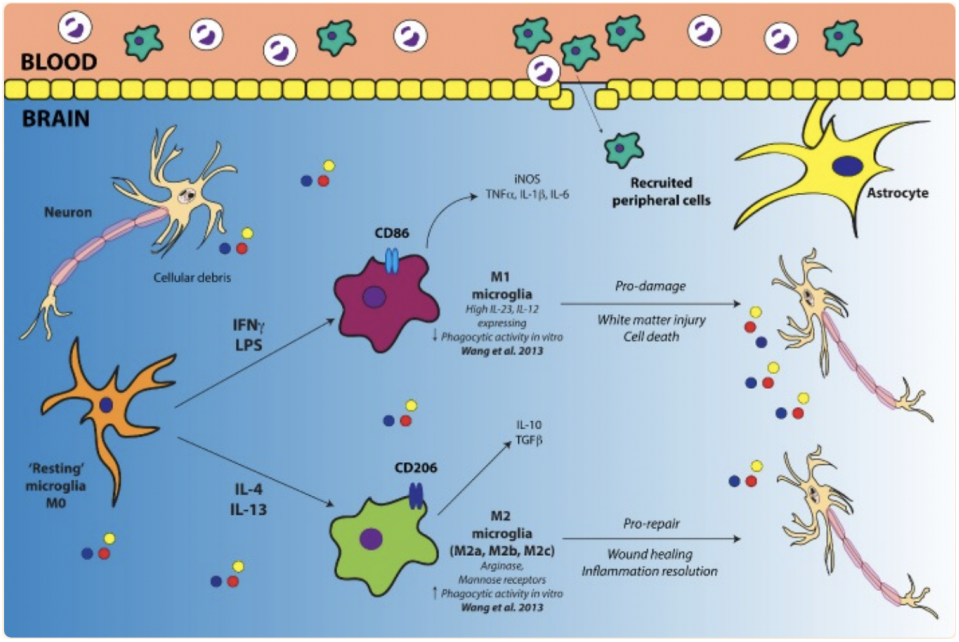

Figure 1: Diagram representing the M1/M2 polarization in microglia. CD86 and CD206 are the only markers labeled here, but there are multiple M1 and M2 markers for microglia. Figure taken from Karve et al.

Microglia play a critical role in the CNS microenvironment as the primary immune effector cells. Microglia have a rod-shaped soma in their resting state, but when activated their soma transforms into a spherical ameboid-like shape and begins to migrate to the injury site (Younger et al., 2019). Activated microglia polarize along an activation spectrum between two phenotypes commonly classified as M1 or M2, which represents its pro-inflammatory and anti-inflammatory states respectively. Similar to macrophages, activated microglia can polarize into multiple phenotypic types depending on the inflammatory stimuli. This means that the microglial response is dependent upon the type, severity and

location of brain injury. M1 microglia are activated in response to TNF-α and IFN-γ, and are known to phagocytose cellular debris as well as secrete superoxide, reactive oxygen species (ROS), nitric oxide, and proinflammatory cytokines and chemokines (Corps et al., 2015; McGinn & Povlishock, 2016). During this time, activated M1 microglia upregulate their cell surface markers such as MHC-II and CD86 (Toledano Furman et al., 2020). Although this M1 activation is to serve a neuroprotective response, a sustained inflammation response can lead to secondary degeneration. This can cause long-term axonal injury and neurological impairments by lipid peroxidation and apoptosis (Fehily & Fitzgerald, 2017). M2 microglia are activated in response to IL-4 or IL-13, and secrete scavenger receptors, growth factors like TGF-β, protein markers like CD206, and anti-inflammatory cytokines like IL-10 (Karve et al., 2016; Loane & Kumar, 2016; Younger et al., 2019). M2 microglia bolsters immunosuppression and manages M1-mediated neuroinflammation, by engaging in CNS remodel and repair via regulating neurorestorative processes including neurogenesis, angiogenesis and remyelination (Loane & Kumar, 2016).

Microglia are known to express a range of ionotropic (P2X4 and P2X7) and metabotropic (P2Y1, P2Y2, and P2Y12) purinergic receptors that play roles in activation, movement, or paracrine signaling (Haynes et al., 2006). Ionized calcium binding adapter molecule 1 (Iba-1) and P2Y12R are markers that are commonly used to study microglia in neuroinflammation (Yip et al., 2022). Iba-1 in particular, is known to be one of the most robust markers for microglia in paraffin-embedded human brain sections, and is useful for 3D analysis because it is uniformly distributed (Sasaki, 2017). However, while Iba-1 is a common marker for both microglia and macrophages, the P2Y12R marker is specific to microglia (Jurga et al., 2020). Thus, this study will use P2Y12R and Iba-1 in combination to distinguish the microglia within the spheroids (Haynes et al., 2006; Nakamura et al., 2013). Moreover, unlike Iba-1, P2Y12 receptor has been reported to be expressed only in the resting (inactivated) microglia (Korzhevskii et al., 2021).

M1 markers for microglia include CD11, CD45, CD32, and CD86 (Toledano Furman et al., 2020). CD86 is a common M1 marker studied because microglia are antigen presenting cells, and when

activated, must communicate with T cells using surface markers like CD86 (Toledano Furman et al., 2020). The number of CD86-positive cells are shown to increase significantly after TBI, and Wen et al. noted a peak in CD86 expression at 72H post-TBI (Peruzzaro et al., 2019; Wen et al., 2018).

Lipopolysaccharides (LPS) are known to induce microglia into an activated state. This state is morphologically characterized by shorter branches and larger cell bodies. Thus, many papers looking at microglial activation often induce microglia activation via LPS treatment (Kumar et al., 2017). Jiang et al. found that LPS specifically promoted the M1 markers for microglia, such as IL-6, TNFα, COX2, and CD86 (Jiang et al., 2021).

Out of the handful of M2 microglia markers including CD163 and Arg-1, CD206 is one of the most typically applied marker in TBI studies (Gensel & Zhang, 2015). For example, Harvey et al. found that CD206 expression increased at 3 days post-TBI and slightly decreased at 7 and 21 days post-TBI (Harvey et al., 2015). CD206 expression in Wang et al.'s paper found that it slightly differed depending on the brain region. In the ipsilateral cortex and striatum, the CD206 expression increased at 3 days post-TBI and peaked on day 5, before decreasing. Similarly in the ipsilateral corpus callosum, CD206 expression peaked between day 3 and day 5. However, in the contralateral corpus callosum, the CD206 was slightly increased after TBI and only on day 3. Thus, Wang et al. concludes that there is a temporary shift from transient M2 microglia phenotype to M1 (Wang et al., 2013).

Similar to how LPS is used to induce M1 microglia, peroxisome proliferator-activated receptor-γ (PPAR-γ) agonists are known for inducing anti-inflammatory effects via PPAR-γ activation. Treatment with rosiglitazone, a PPAR-γ agonist, has been shown in various TBI studies to decrease the production of inflammatory cytokines after TBI, and reduce overall neuronal apoptosis and autophagy (Yao et al., 2015; Yi et al., 2008; Zhang et al., 2010). Furthermore, Peng et al. found that rosiglitazone treatment increased the expression of M2 marker CD206 and decreased the M1 marker CD86 in the TBI group (Peng et al., 2019). Thus, in this study, rosiglitazone and LPS treatment will also be examined.

Models of TBI

There are many challenges to modeling TBI as no single model can fully simulate all of the primary and secondary damages that occur in human TBI, including the diverse injury mechanisms that determine the patient's outcome (Jassam et al., 2017).

Although two-dimensional (2D) models of the brain are popular in studying cell-cell interactions, there are several limitations, such as providing a simplified depiction of the brain that fails to capture the complex structures and its unique functions (Jorfi et al., 2018). Three-dimensional (3D) models are increasingly popular due to the growing number of technologies available such as biomaterials and microfabrication techniques. 3D models have been demonstrated to have physiological relevant models that closely resemble the human nervous system by simulating spatial organization, cell diversity, and cell-cell and cell-extracellular matrix interactions (Ryu et al., 2019; Sloan et al., 2018). While cell-seeded scaffolds are prevalent in many CNS studies, spheroids provide a more favorable cell microenvironment and increased cell density (Fennema et al., 2013). Spheroids express adherens junction-associated proteins, tight junctions, adherens junctions, and cell specific markers (Nzou et al., 2018). Rodent models are most often used in TBI research because of their accessibility, low cost, small size, and physiological similarity to humans (Marklund, 2016). However, some animal models have limitations with structural changes in the brain that weren't present in clinical TBI, or modified TBI pathophysiology and outcomes due to anesthetics or craniotomy used in the study (Pham et al., 2021).

The Hoffman-Kim laboratory thus created a model that combines the rodent model with the spheroid model, and produced 3D neural spheroids from postnatal primary rat cortical tissues. The method only requires commercially available culture materials and can be done in a standard laboratory setting with conventional biomaterial techniques, thus making the protocol easily reproducible. This cortical neural spheroid contains neurons, glia and cell-synthesized matrix while having mechanically similar properties to *in vivo* cortex and being electrically active (Dingle et al., 2015).

Mode of injury

TBI can be caused by blunt impacts, penetrating impacts, non-impact blast waves, or inertial loading (Fehily & Fitzgerald, 2017). These injuries produce mechanical forces such as acceleration and deceleration linear forces, rotational forces, forces caused by blast winds in blast injury, blunt impact, and penetration. These forces then damage the neurons, axons, dendrites, glia and blood vessels in a series of cascades that develop into secondary injuries. Out of these forces, humans are especially susceptible to brain damage associated with rotation and linear-acceleration-deceleration forces due to the ratio of the size and weight of the brain to the body, large amounts of white matter relative to gray matter, and its gyrencephalic composition ((Johnson et al., 2013; Mckee & Daneshvar, 2015). Specifically, rotational acceleration is known to cause diffuse axonal injury (DAI), which is a universal injury across all severities of TBI (Fehily & Fitzgerald, 2017; Humble et al., 2018).

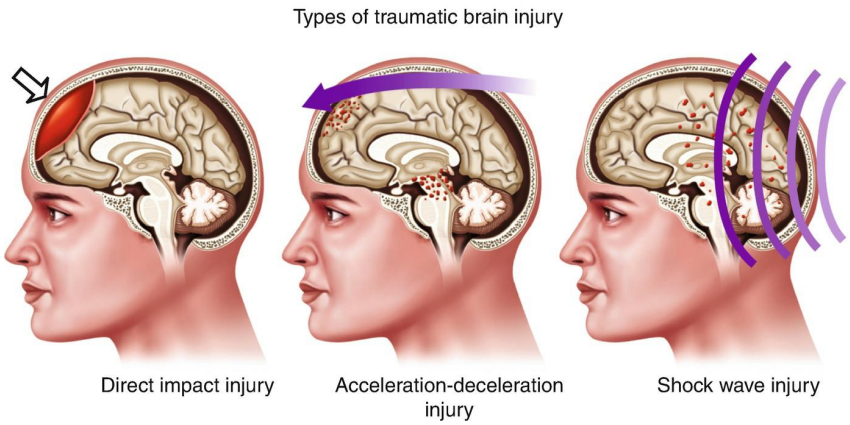

Figure 2: Representative images of three major types of traumatic brain injury. The forces resulting from the injury result in primary and secondary injuries to the brain. Image from Suer and Abd-Elsayed

Repeated mTBIs are common in sports and military activities, and can create prolonged symptoms that affect quality of life for athletes and military personnel. However, there is a huge lack of studies examining the pathophysiology of repeated mTBIs ((Bolton-Hall et al., 2019; Feng et al., 2021). Clinical research has shown that three or more mTBIs in athletes and military personnel results in a

significant impact on the susceptibility and outcome of these injuries. Three repeated mTBIs have been reported to increase susceptibility to another mTBI by three to nine times. Additionally, three repeated mTBIs can culminate in a longer loss of consciousness time and the longer-lasting TBI symptoms(Nichols et al., 2016). Repeated mTBI is also associated with permanent sensorimotor, cognitive, and behavioral deficits, as well as progressive neurodegeneration and functional decline (Broussard et al., 2018). It has reached a point that the US Department of Defense has implemented a "three-strike" policy in that individuals who experience a third mTBI must be removed from the environment where the injury took place (Adams et al., 2018).

Research Aims

This study's research goal was to develop an *in vitro* 3D brain model that characterizes neuroinflammation after single and repeated mTBIs. 3D cortical spheroids from the Hoffman-Kim laboratory were used in this study as an *in vitro* brain model, from which neuroinflammatory biomarkers were assessed at multiple time points depending on injury frequency and treatments. Before addressing each of the aims in the study, a 2D antibody dilution test was needed to determine the optimal dilution factors for each of the markers for the spheroid model used in this paper. After determining the optimal dilutions, that dilution factor was used to stain the 3D spheroid culture for the aims described below.

The first aim of the study was to characterize the M1/M2 phenotype that was present in cortical spheroids at resting state. The resting microglia was stained in 3 sets: (1) P2Y12R , Iba, DAPI (2) CD86, Iba, DAPI, (3)CD206, Iba, DAPI. For this aim, it was expected that P2Y12R will have the greatest expression, and there would be low expression of the activated microglia markers, CD86 and CD206 (Korzhevskii et al., 2021).

The second aim was to characterize M1/M2 phenotype present in cortical spheroids after single and repeated mTBI. The spheroids were injured via centrifugation at 4000 RPM for 2 minutes. The measured time points were: immediately after injury, 24H after injury, 3 days post-injury, 5 days

post-injury, and 7 days post-injury. Before this second aim was conducted, the M1 phenotype was measured using LPS stimulation. Both M1 and M2 marker expression was expected to increase after injury, with the M2 expression being transient and M1 expression having a sustained expression until 7 days (Peruzzaro et al., 2019; Wang et al., 2013; Wen et al., 2018).

The third aim was to induce M2 phenotype after repeated mTBI with pharmacological agents, rosiglitazone, and measuring neuroinflammation to see therapeutic effects. For this aim, it was expected that the M2 marker expression will increase, with a decrease in M1 marker expressions (Peng et al., 2019).

Methods

Cell Isolation and Culture

CD Sprague Dawley IGS rats from Charles River Laboratories were used in this study (Wilmington, MA). Cell isolation protocol was altered from the BrainBits protocol. Rat cortical tissues were sliced into parts and placed in papain solution at 30℃ for 30 minutes. Hibernate A, 1xB27 supplement, and 0.5 mM GlutaMAX were combined to prepare Hibernate A buffer solution. The tissue was taken out of the papain solution and titrated with fire-polished Pasteur pipettes 20 times in Hibernate A buffer solution. The solution was then centrifuged at 150g for 5 minutes. After centrifugation, the supernatant was removed, and the cell pellet was resuspended in Complete Cortical Medium (CCM). CCM was composed of Neurobasal A medium, 1xB27, 0.5mM GlutaMAX, and 1x Penicillin-Streptomycin. The solution was passed through a 40μm cell strainer, and then washed by centrifuging at 150 g for 5 minutes. The cell pellet was then resuspended in Neurobasal A/B27 medium, and the cell solution was filtered through a cell strainer. Cell viability was calculated using Trypan Blue Exclusion Assay (Invitrogen) and a microscope. The cortical cells were seeded at a density of 4000 cells/spheroid and maintained by exchanging the CCM every 2-3 days.

3D Cortical Spheroid Culture

The 3D rat cortical spheroids were formed using 96 well agarose gels with round-bottomed microwells using a protocol developed from a member of the lab (Dingle et al., 2015). The agarose gels were obtained by pouring molten 2% agarose (Invitrogen) solution onto a spheroid micromold with 400 µm diameter round pegs (#24-06 Small, MicroTissues, Inc). Agarose gels were brought to equilibrium in culture medium and maintained by changing the media three times over a 48 hour time period. Cortical cell solution was centrifuged and resuspended in Neurobasal A/B27 medium. The media was aspirated from the gells, and the cell solution was seeded at 75 µL/gel. After letting the cells settle into the microwells for 30 minutes, 1 mL of Neurobasal A/B27 medium was added into each gel. The spheroid culture was then preserved by exchanging the media after 48 hours and after every 2-3 days (Dingle et al., 2015).

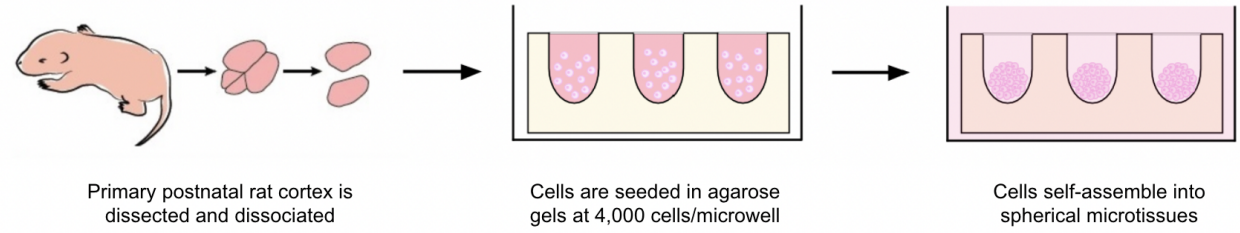

Figure 3: Diagram of 3D cortical spheroid culture assembly. The rat cortex is dissected from primary postnatal rats and seeded into agarose gels, where they self-assemble into spheroids.

2D Antibody Dilution

To test the optimal dilutions for the antibodies and drugs for the spheroids, a series of dilutions were tested in 2D control cells. For the activated microglial markers, either LPS or rosiglitazone was inserted into each of the dilution wells, and removed after 24H. Working solution was prepared by combining 1 ml of 100% normal goat serum, 0.2g of bovine serum albumin (BSA), and 19 ml of PBS.

Blocking solution was prepared by combining 100 ul of 10% Triton-X100 and 4.9 ml of working solution. PBS was removed from each well and the cells were blocked with 1 ml of blocking solution for 1 hour. Meanwhile, the primary antibody was diluted in working solution for a volume of 0.5 ml per well for the following dilutions: 1:50, 1:100, 1:200, and 1:500. Depending on the antibody or drug, there was a positive control well with a dilution of 1:100. After blocking, the blocking solution was removed and 0.5 ml of the diluted primary antibody was added to each of the wells. The plate was then sealed with parafilm and stored in 4℃. The following day, the primary antibody solution was removed from the wells and stored in tubes in the 4℃ refrigerator. Each well was washed with 2 ml PBS 3 times, with 10 minutes between each wash. Meanwhile, the secondary antibodies (CY3 and AlexaFluor 488) were diluted with working solution at 1:500. After removing PBS, the wells were washed with 1 ml of working solution for 10 minutes. The working solution was removed, and 0.5 ml of the diluted secondary antibody solution was added to each well. The plate was covered with foil and left at room temperature for 1 hour. The secondary antibody solution was then removed and each well was washed with 2 ml of PBS 3 times. Meanwhile, DAPI was diluted with PBS at 1:100 dilution. After PBS washing was finished, 1 ml of the diluted DAPI solution was added to each well. The plate was covered with foil and let sit at room temperature for 10-15 minutes. The DAPI solution was then removed and 1 ml of PBS was added to each well. The plates were then sealed with parafilm and covered with foil, before storing it at 4℃.

Centrifugation Injury

On DIV14, complete cortical media was warmed at 37℃ for about 20-30 minutes. Meanwhile, the gels for injury conditions were moved to separate plates depending on the condition. The gels were placed on the same locations on the plate, so as to ensure that the plates would be balanced in the centrifuge. Being careful not to disturb the spheroids in the gels, CCM was removed from each well, and 1 mL of the warmed CCM inserted into the wells. If there was a well that was not balanced, an empty gel and 1 mL of PBS was added. The plates were then carried in a styrofoam box to the centrifuge. The

spheroids were then subjected to centrifugation injury at a centrifugation speed of 4000 RPM for 2 minutes at acceleration and deceleration settings at 9. For consecutive repeated injuries, the lid was opened briefly after the end of 2 minutes, before starting the centrifugation again. The injuries were either a single injury or three consecutive injuries. The gels were then taken back to the incubator and maintained until they were fixed at either 0H post-injury, 24H post-injury, 3 days post-injury, 5 days post-injury or 7 days post-injury. The gels were fixed by removing CCM and inserting 1 ml 4% paraformaldehyde/8% sucrose solution in the wells overnight. The next day, the paraformaldehyde was removed and the wells were washed with PBS three times. For 2D cells, there was 10 minutes between washes and for 3D spheroids, there was 30 minutes between washes. After the washes, PBS was inserted into the wells and the plates were wrapped in parafilm and stored at 4℃.

LPS and Rosiglitazone Exposure

LPS dilution in this spheroid model has been previously determined by experiments conducted by researchers in the Borton Lab at Brown University (Atherton et al., 2021). To calculate for 5 ml of diluted LPS was as follows:

$(\frac{1000\,ug}{ml})x \;=\; (\frac{10\,ug}{ml})(5\,ml) \rightarrow$ x = 0.05 ml = 50 ul of 1 mg/ml LPS in 5 ml of CCM

At DIV14, the CCM was carefully removed from the LPS wells so as not to disturb the spheroids in the gels. 1 ml of LPS diluted in CCM was then inserted into each well. The media was removed 3 days later, and the spheroids were fixed in the same process as explained above.

For rosiglitazone exposure, the 10 mg/ml solid stock was dissolved in DMSO to get a concentration of 28mM. 35 ul of the 28mM stock was then added to 1 mL of media to be diluted to a concentration of 1mM. 1ul was removed and inserted into 999 ul of CCM and warmed in 37℃ to get a final concentration of 1 μM. The media in the wells were removed, before inserting the 1 ml of 1uM

rosiglitazone into the well. Rosiglitazone+CCM mixture was exchanged every 2-3 days until the day of fixation for the spheroids.

Immunohistochemistry

Overview of IHC protocol: IHC is a staining technique that is used to detect the presence of specific proteins. The sample is first fixed in order to preserve the antigens of the proteins of interest and also prevents autolysis or necrosis. The sample is then blocked to prevent non-specific binding of antibodies to the spheroids. The primary antibody is added to bind to the antigens on the protein of interest. The sample is washed in order to remove unbound antibodies and remove antibodies that may be attached to nonspecific sites. A secondary antibody that is fluorochrome labeled is then attached to the primary antibody. It is important to note that the secondary antibody species must be anti to the primary antibody species to prevent cross-reactivity. The samples are then visualized by a confocal microscope.

Day 1: Preparation of samples and blocking and primary antibody staining

On the first day of the IHC protocol, the samples were taken out of the fridge and PBS was removed from each of the samples. The spheroids were removed from the gels by pipetting 1ml of PBS into the gels. After cutting the tip of the pipette to prevent damaging the spheroids, the 1mL in the well was pipetted up and used to flush the spheroids out of the gels. To confirm that the majority of the spheroids had been removed, a light microscope was used to check how many spheroids remained in the gels. If most of the spheroids were removed, the 1mL of PBS and spheroids were transferred into an Eppendorf tube. Once all the spheroids from each experimental group were transferred into the Eppendorf tubes, the tubes were left for 5 minutes to let the spheroids settle to the bottom of the tube. PBS was carefully removed without removing any spheroids. 1 mL of blocking solution was added to each of the tubes. 50mL of blocking solution is made up of 400 mL of PBS, 5mL of normal goat serum, 5mL of 10% Triton X, and 2g of Bovine serum albumin (BSA). Triton X is important as it disrupts the cell membrane, making the cells

more permeable for antibody attachment. Blocking solution is necessary to prevent nonspecific binding of the antibodies to the sample. Thus, this makes sure that the antibodies attach only to the protein of interest. The samples were then placed on a shaker at room temperature and at 90 rotations per minute (RPM) for 2 hours. During the 2 hours, the primary antibody solution was diluted with blocking solution at ratios listed above to create the primary solutions. After 2 hours, the blocking solution was then removed and 1mL of the diluted primary antibody solutions were added to each of the samples except for the control sample, where 1mL of blocking solution was inserted instead. The tubes were closed and wrapped with parafilm, and placed on the shaker at 90 RPM overnight.

Day 2: Blocking and secondary antibody staining

The samples were taken off the shaker and left to let the spheroids settle to the bottom of the tubes. After 5 minutes, the primary antibodies were removed from each of the samples without disturbing the spheroids at the bottom. The samples were then washed quickly with 1 mL of PBT. 1 mL of PBT was added and placed on the shaker at 90 RPM and at room temperature for 2 hours. This step was repeated again for another 2 hours. The samples were then washed with blocking solution and placed on the shaker for another 2 hours. The secondary antibody solutions were diluted at 1:500 dilution. The secondary antibody solutions consisted of 10 uL of AlexaFluor goat anti-mouse and 10 uL of CY3 anti-rabbit, and 4980 uL of blocking solution. After the 2 hours, the blocking solution was removed and 1 mL of the diluted secondary antibody solution was added to each of the wells. The plate was then wrapped with tin foil to prevent exposure to light and placed on the shaker overnight.

Day 3 of IHC:

On the third day, the samples were taken off the shaker and left to settle the spheroids. After 5 minutes, the diluted secondary antibody solution was removed. The spheroids were then washed with PBT two times for 2 hours each time and placed on the shaker. DAPI was then diluted in PBT in a 1:100 ratio, where 50uL of DAPI was inserted into 5mL of PBT. After the second PBT wash, PBT was removed from each of the wells, and 1 ml of the diluted DAPI was added to each well. The plate was then covered with foil and placed on the shaker for 1 hour. After 1 hour, the DAPI was removed and 1 mL of PBS was added to each well. The spheroids were then placed in the fridge until ready for imaging.

Imaging

The 2D cells and 3D spheroids were imaged using Olympus FV 3000 Confocal Laser Scanning Microscope. Galvano scanner was selected, and for 2D the Z-range was turned off. For 3D, images of 50 slices of 1.5µm apart were taken using the Z-range. The first channel was DAPI, the second channel was AlexaFluor488, and the third channel was CY3 to obtain the images.

ImageJ analysis

To analyze the confocal images, the software program Fiji, distributed by ImageJ, was used. The spheroids were analyzed either via 3D object count protocol (3DOC) or using the 3D Filter → 3DOC tools.

Converting OIR files into Tiff files

First, the OIR files were converted to Tiff files. The OIR file was dragged right into ImageJ, and the settings for the file format were set as shown below.

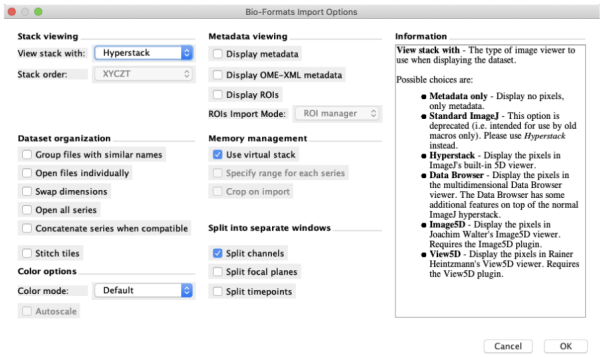

Figure 4: File settings when opening the OIR file in ImageJ

The file will open up with three separate channels, one for each of the dyes. Each channel was saved as an Image Sequence between 1-50 slices into a newly created folder that labeled the date, injury condition, dye, and spheroid number.

Determining the threshold for the 3D Object Counting Algorithm

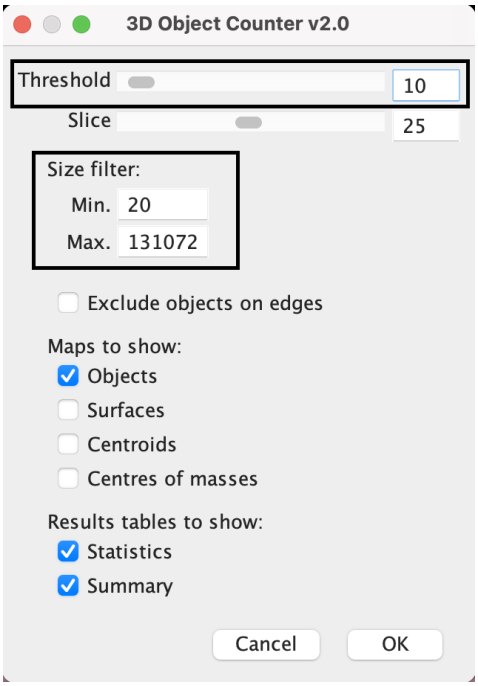

Figure 5: Threshold and size filter settings for 3D Object Counter Plugin. The optimal threshold and size settings were determined by testing a range of values and comparing the outputs to the original Tiff files and the z-stack images.

In order to identify the microglia within the spheroids, the 3D Object Counting algorithm requires a pixel threshold value and size to be set (Fig.5). The pixel values range from 0 to 1023, where 0 is the dimmest pixel and 1023 is the highest pixel. By setting a threshold value, the algorithm determines which pixels in the image are high enough to be classified as objects, and which pixels are background. The size limit with the minimum and maximum values determine what range of pixel sizes are to be counted as an object instead of background. To determine the optimal threshold for the confocal images, one image from each condition was downloaded. The tiff file was converted to 8-bit, and the image properties were set to 0.829, 0,829, 1.5 um for the pixel height, pixel width, and voxel depth. Images were cropped using the ellipse selection tool to ensure that only one spheroid was present per field of view. The z-stack image of the Tiff file was taken, and the z-stack images were labeled and put into a word document for easy side-by-side comparison. The Tiff files were then tested for varying thresholds and sizes by running the 3D Object Counter plugin, to ensure that the optimal number of microglia were identified. The z-stack images of each tested threshold were compared to the original z-stack image to determine the optimal thresholds. The plugin also outputs an object map, which is a 3D stack file of all of the objects that the 3DOC plugin identifies. This file was also scrolled through all 50 slices and compared to the 50 slices of the original file, to check that no objects were double counted and that the microglia were segmented from each other and identified separately. This process was conducted for both the CD206 and the P2Y12 data. The optimal threshold and size filters were found to be 80 and 30, 10 and 20 respectively.

3D Edge and Symmetry Filter

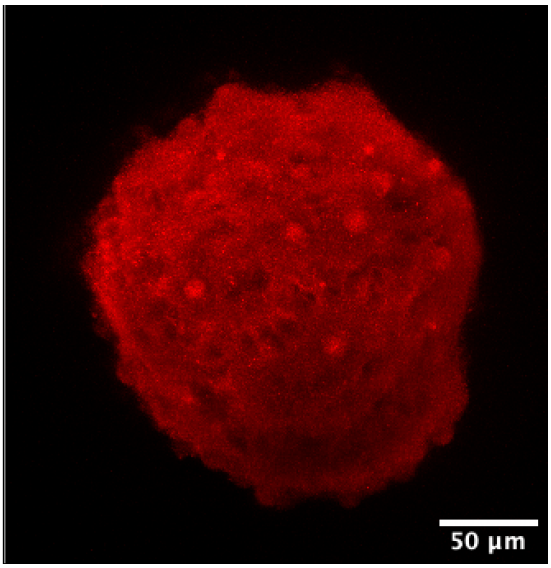

Figure 6: A number of conditions for the CD206 staining, produced images with overlapping microglia and considerable background. This is a representative image of spheroid #3 stained for CD206 for injury condition 4kRPMx3 7DPI

For the CD206 confocal data, there were a number of conditions that produced images with overlapping microglia and a lot of background as shown in Figure 6. Thus, a 3D Edge and Symmetry Filter under the 3DSuite plugin was used to distinguish between the microglia. This plugin uses the Canny edge detector algorithm to compute the gradients of the voxels in the image to identify objects. The file was first converted to 8-bit, the properties were set to the same parameters as stated earlier, and the image was cropped to fit only one spheroid per view. The edge filter was then selected and the parameters for the filter were set as shown in Figure 7. The symmetry output was then converted to 8-bit and run through the 3DOC plugin.

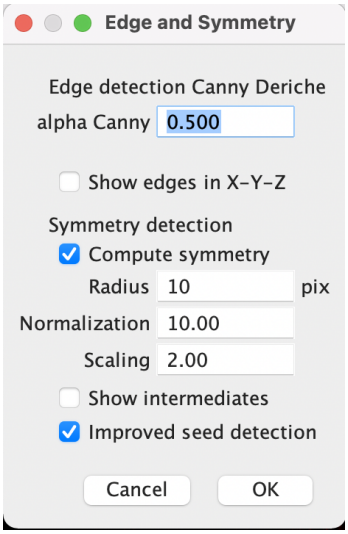

Figure 7: Edge and Symmetry Filter parameters used when analyzing CD206 data

3D Object Counting Algorithm

The 3DOC plugin was used to analyze both the CD206 and the P2Y12 data. For the P2Y12 data, the original 50 stacked Tiff image was analyzed, whereas for the CD206 data the symmetry output from the 3D Edge and Symmetry Filter was analyzed using the 3DOC algorithm. The image was converted to 8-bit grayscale image stack and the image properties were again confirmed to be set to 0.829, 0.829 and 1.5 um for pixel height, pixel width, and voxel depth respectively. The file was checked to ensure that only one spheroid was in the field of view and if not, was cropped using the ellipse selection tool. The 3D Object Counter plugin parameters were selected by going to Analyze → 3D OC Options. The following parameters were calculated by the plugin and the descriptions of the parameters are adapted from the ImageJ documentation provided by ImageJ (*3D Objects Counter*, 2009).

Parameter	Parameter Description
Volume	Number of voxels (volume picture element) of the object × x calibration × y calibration × z

	calibration
Number of object's voxels	The number of voxels that is part of the object
Surface	Identifies the surface of the object by considering the differences of dimensions between the xy, xz, and yz sides of the surface voxels
Integrated density	Sum of all the voxel's intensities for each object
Mean of gray value	Average of the all the voxels' intensities for each object

Table 1: The parameters measured using the ImageJ 3D Object Counter plugin

The plugin was run by clicking on 3D Object Counter under Analyze. The optimal threshold and size values were inputted into the plugin as previously determined. Objects and Statistics were selected to produce a 3D image stack of all the identified objects and their counts, as well as a datasheet with all the measurements generated about each object identified. The data from the Statistics table was copied and pasted into a separate excel file for further calculations. To adjust the brightness of the object map, the Brightness and Contrast was selected under Image, and the Maximum bar was dragged to the left until all objects were clearly recognizable.

Calculations for Total Mean Pixel Intensity and Sphericity

Using the parameters collected from the 3D Object Counter, the following values were calculated for further analysis: sphericity for P2Y12 data and total mean intensity for both CD206 and P2Y12R . The sphericity values for CD206 were not collected because of two reasons. First, the CD206 data was analyzed using the Edge and Symmetry Filter, which slightly alters the shape of the object for easier

detection. Secondly, CD206 can also be released by other cells and is not limited to microglia, and for this study, the microglia was the main focus.

To calculate the overall mean intensity per spheroid, the weighted average of the individual mean intensities per object in each spheroid was calculated. This was done using the outputs of the 3D OC plugin. After running the plugin, one of the outputs is a Summary table that incudes a mean of gray value for each object, which is the mean intensity of each object. The sum of the mean intensity of each object is multiplied by the object size (the number of object voxels), and then divided by the sum of the total number of object voxels in the spheroid. This calculation was done for each of the 10 spheroids that were imaged per condition. The total mean intensity is a useful measurement to compare the relative brightness of the expression of CD206 and P2Y12Ron microglia between conditions. A example calculation is shown below:

Object Number	Nb of Obj Voxels	Mean Gray Value
Obj 1	157	15.395
Obj 2	113	13.628
Obj 3	205	14.849

$$Total\ mean\ intensity\ of\ each\ spheroid\ = \frac{\{(157*15.395) + (113*13.628) + (205 * 14.849)\}}{157+113+205} = 14.739$$

Figure 8: Example Calculation of the Overall Mean Intensity Per Spheroid

To determine the overall shape of the microglia objects, a total sphericity value for each spheroid was calculated using the 3DOC outputs: Volume, Surface Area, and Nb. Obj Voxels. The sphericity

values range between 0 and 1, where 1 equates to a perfect sphere and 0 equates to an elongated shape. The overall sphericity value for each spheroid was calculated using the weighted average of sphericity values for all of the microglia objects. This calculation was again repeated for all 10 spheroids per condition. An example calculation is shown in Figure 9:

Object Number	Volume (µm^3)	Surface Area (µm^2)	Nb. Obj Voxels
Obj 1	41.199	180.08	40
Obj 2	66.948	282.123	65
Obj 3	232.773	449.062	226

$$Sphericity\ of\ an\ object\ = \frac{\sqrt[3]{36\pi V^2}}{S}$$

$$Weight\ = Nb.\ Obj\ Voxels/Sum\ of\ Obj.\ Voxels$$

$$Weight - adjusted\ Sphericity\ = Raw\ sphericity\ * Weight$$

$$Total\ Sphericity\ = Sum\ of\ weight - adjusted\ sphericities$$

Weight	Unweighted Sphericity	Weight-Adjusted Sphericity
0.1208	0.3203	0.0387
0.1964	0.2826	0.0555
0.6828	0.4075	0.2782

$$Total\ Sphericity\ = 0.0387\ +\ 0.0555\ +\ 0.2782\ =\ 0.3724$$

Figure 9: Example Calculation of Total Sphericity per Spheroid

Statistics and graphs

The statistics for the data were analyzed using JMP Pro 16, and the graphs were produced using GraphPad Prism 9. The data was first tested for normality using the Shapiro Wilk test with a significance level of 0.05 using the Distribution tool. It was then tested for equal variances with a significance level of 0.05 by using the unequal variance tool on the Fit Y by X analysis, which displayed 4 p-values for the following variance tests: O'Brien, Brown-Forsythe, Levene, and Bartlett. If the data passed both the normality and variance tests, then the ANOVA test was run to test for significance. If the data was significant, then the post-hoc Tukey Test was run to determine which pair comparison had significant data. If the data passed normality but failed the variance test, the Welch's test was run to test for significance using Bonferroni adjustments. If the data failed normality but passed the variance test, the Wilcoxon/Kruskal Wallis Test was run to test for significance. If it passed, the Steel-Dwass test was run with no Bonferroni adjustments. If the data failed both normality and variance tests, the median test was run on all of the data and also on each of the comparisons using Bonferroni adjustments to determine significance between groups. The Bonferroni adjusted alpha is calculated by dividing 0.05 by the number of comparisons. For example, if 4 total comparisons are being made, then the new Bonferroni adjusted alpha is:

$$0.05 \,/\, \#\, of\ comparisons \;=\; 0.05/4 \;=\; 0.0125.$$

Results

2D Dilution Testing for CD86

A	CD86 (LPS-treated)					
DAPI (1 ug/ml) + Iba1 (1:200)	1:50	1:100	1:200	1:500	Control (No LPS)	No Primary Control

B	CD86 (control)					
DAPI (1 ug/ml) + Iba1 (1:200)	1:50	1:100	1:200	1:500	LPS 1:100	No Primary Control

Table 2: 2D dilution testing conditions for CD86 marker A) 2D plate to test antibody dilutions for CD86 using LPS treated cells B) 2D plate to test for antibody dilutions for CD86 with no treatments

First, 2D antibody dilutions for CD86 were tested as described in the Methods in order to determine the optimal antibody dilution. In one plate, 4 wells were treated with LPS and tested dilutions with a range between 1:50 and 1:500. The CD86 antibody was co-stained with DAPI and rabbit-against Iba-1 which both have been previously used in the lab. At all dilution concentrations in the two plates, the DAPI and Iba-1 staining was present, but CD86 antibody was not detected at control or LPS treated conditions (Figure 10).

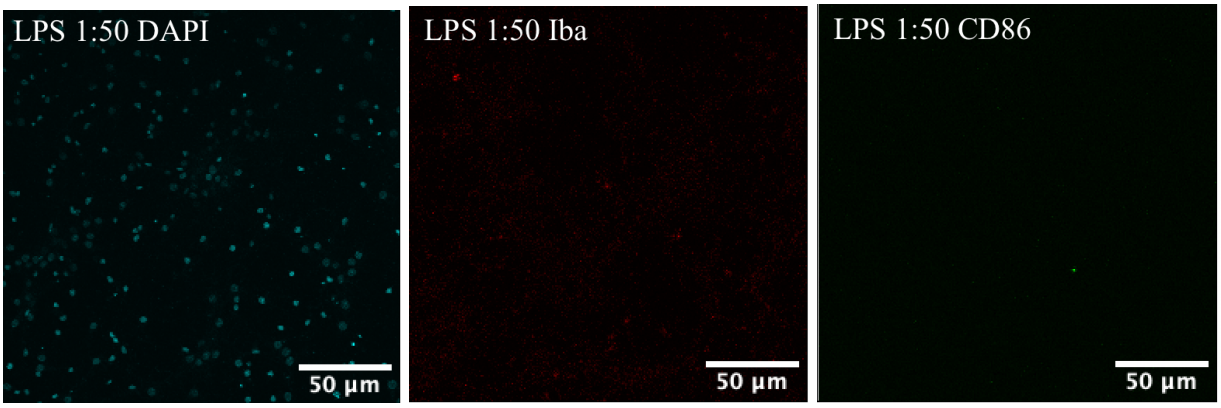

Figure 10: No CD86 was detected at any of the 2D conditions that were tested. LPS treated 2D control well for 1:50 dilution. From left to right: DAPI staining, Iba-1 staining, and CD86 staining

3D Experiments for CD86 and CD16

While 2D antibody dilutions were being conducted, 3D experiments for CD86 were tested at the same time. The following conditions were tested and stained with CD86, Iba-1, and DAPI with a 1:100 dilution for CD86.

Condition	**Number of gels**
No primary control	1
Control	1
24H exposure to LPS	1
4kRPMx1 7DPI	2 gels

Table 3: 3D injury conditions stained for CD86, Iba-1, and DAPI

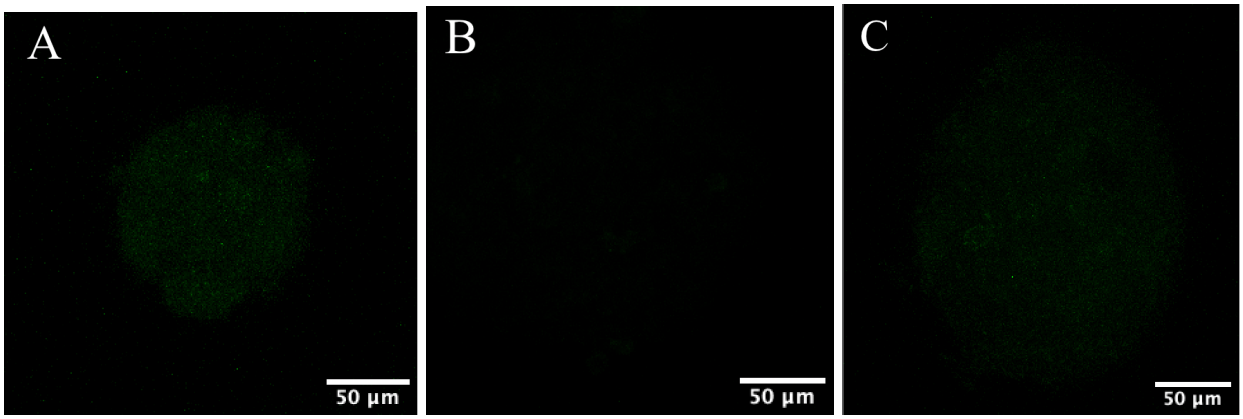

Figure 11: No CD86 was detected for the first set of the 3D experimental conditions. Z-stack images of spheroids stained for CD86 A) Control with no treatment B) 24H LPS exposure C) 4kRPMx1 7DPI stained

However, CD86 was not detected for any of the conditions as seen in Figure 11. The LPS exposure time, injury time-point, and injury severity were three possible factors that were hypothesized to be the reasoning behind the lack of detection. First, the LPS exposure was extended from 24-hour exposure to a 3 day exposure protocol for the positive control, because 3D models using LPS had longer exposure times compared to 2D models. For example, most papers using 2D cell cultures had a LPS exposure time of around 24 hours or less, whereas most papers using spheroid models had a longer LPS exposure time of 2-3 days (Dean et al., 2010; He et al., 2021; Ji et al., 2018; Jiang et al., 2021; Li et al., 2020; Liu et al., 2011). Some TBI papers also saw CD86 expression peak at earlier time points such as at 36 hours post-injury, so earlier time points were also measured (Peruzzaro et al., 2019). Thus, for the next set of spheroids the following conditions were tested and stained for CD86, Iba-1, and DAPI.

Condition	**Number of gels**
No Primary control	1
Control	1
LPS(3 day treatment) 24H	2
LPS(3 day treatment) 5DPI	2
4KRPMx1 5DPI	1
4kRPMx1 7DPI	1
4kRPMx3 5DPI	1
4kRPMx3 7DPI	1

Table 4: Second set of 3D injury conditions stained for CD86, Iba-1, and DAPI

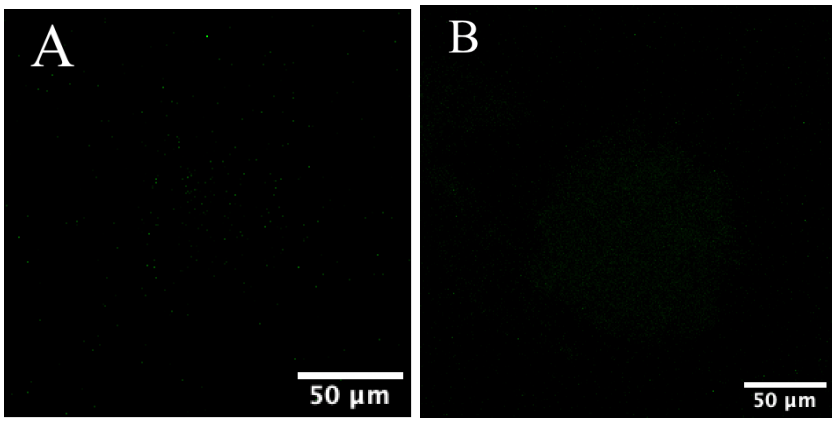

Figure 12: The second set of 3D injury conditions stained for spheroids for CD86

Z-stack images of the spheroids stained for CD86 A) 4kRPMx3 at 5DPI B) 3 day LPS exposure fixed at 5 days

Nonetheless, CD86 was also not detected for this next set of conditions with 1:100 dilution. Thus, another biomarker was researched to test for M1 microglia instead of CD86. After some extensive literature review, CD16 was chosen as a second marker to test for M1 microglia, as it was a common marker studied in inflammatory microglial studies (Kumar et al., 2016). Due to issues with the 2D control cells' low viability, the 2D antibody dilutions for CD16 were discarded and a relatively low dilution of 1:50 for CD16 was used to stain the spheroids. 1:50 was used because it is a particularly low dilution that generally produces a strong staining. The following injury conditions were then tested for CD16 at 1:50 dilution:

Conditions	**Number of gels**
No primary	1 gel
Control	1 gel

LPS (3 day exposure)	1 gel
4kRPMx3 3DPI	1 gel
4kRPMx3 5DPI	1 gel
4kRPMx3 7DPI	1 gel

Table 5: 3D Injury conditions stained with CD16, Iba-1, DAPI

On the 4th day post-injury, immunohistochemistry was conducted on the no primary, control, LPS and 4kRPMx3 3DPI gels and CD16 was not detected using confocal imaging. Thus, the rest of the gels (5DPI and 7DPI gels) were stained with P2Y12 instead of CD16 and will be described further in later sections.

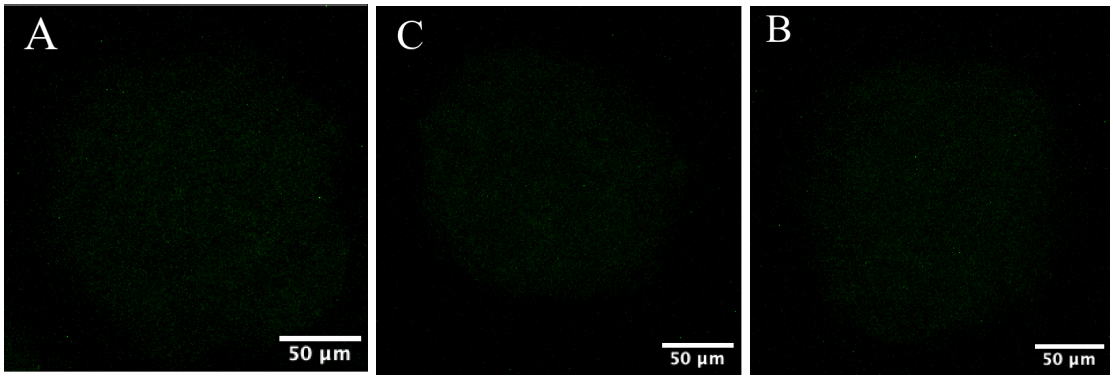

Figure 13: CD16 was also not detected for the 3D injury conditions tested. Z-stack images of spheroids stained for CD16 A) Control with no treatment B) 4kRPM x3 3 days post-injury C) 3 day exposure to LPS

2D Antibody Dilutions for Iba-1, P2Y12R, CD206

2D dilution tests for Iba-1, P2Y12R , and CD206 were also performed with the following dilutions as displayed in Table 6. The Iba-1 antibody for this dilution test was different from the Iba-1 antibody previously used to double-stain with CD86 and CD16, because the host species for this test was mouse whereas the prior one utilized was rabbit. This is important to distinguish because if the host species of two markers are the same, they will cross-react and will not be discernible after the staining is complete.

A	Mouse against Iba1					
DAPI(1 ug/ml)	1:50	1:100	1:200	1:500	LPS :100	No primary

B	Rabbit against P2Y12R R					
DAPI(1 ug/ml)	1:50	1:100	1:200	1:500	LPS:100	No primary

C	Rabbit against CD206					
DAPI(1 ug/ml)	1:50	1:100	1:200	1:500	Rosiglitazone 1:100	No primary

Table 6: 2D plates tested with various antibody dilutions for Iba-1, P2Y12R R, and CD206 to determine the optimal dilution A) Antibody dilutions for Iba-1 using LPS as a positive control B) Antibody dilutions for P2Y12 with LPS used as positive control C) Antibody dilutions for CD206 with rosiglitazone as a positive control

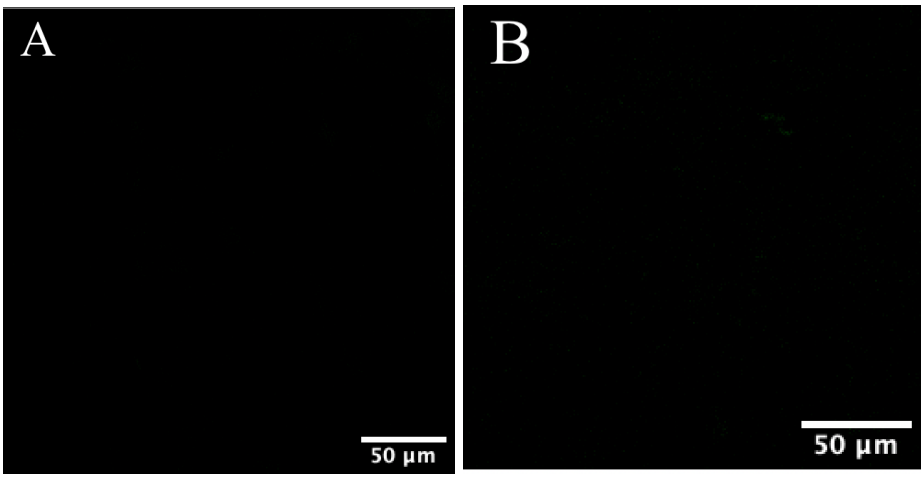

Figure 14: Mouse against Iba-1 is not detected as seen by confocal images of 2D antibody dilutions

A) No treatment with 1:50 dilution B) LPS treatment with 1:100 dilution

For these 2D dilution tests, mouse against Iba-1 was not detected at any of the dilutions tested. Thus, mouse-against Iba-1 was discontinued for future stainings, and rabbit-against Iba-1 was utilized for immunohistochemistry.

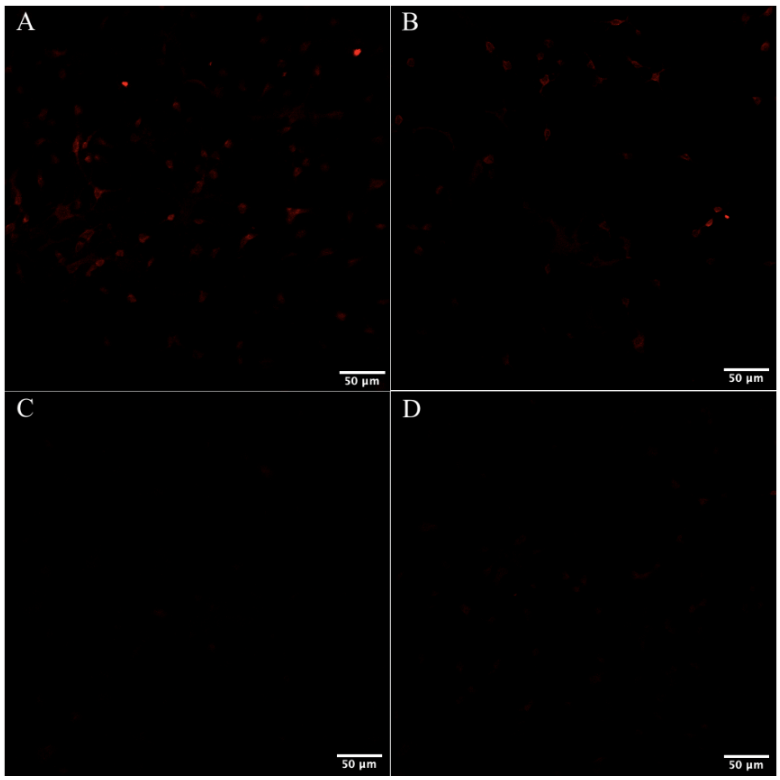

Figure 15: Confocal images of 2D Antibody Dilutions revealed that 1:50 dilution of P2Y12Ris the optimal dilution A) 1:50 dilution B) 1:100 dilution C) 1:200 Dilution D) 1:500 dilution

Examining the four 2D dilutions tested for P2Y12R , 1:50 dilution was found to be the optimal dilution as it had the strongest signal as shown in Figure 15. The 1:200 and 1:500 dilutions are very faint and difficult to detect (Figure 15 C and D). The 2D cells used for the 2D dilution tests for CD206 were taken from the same dissection as the CD16 set, so similarly, the 2D dilution plate for CD206 had to be discarded and could not be stained.

Mean Pixel Intensities for CD206

Due to the inability to test for 2D antibody dilutions for CD206, the first set of spheroids had to be stained for CD206 without prior confirmation of the optimal dilution. Thus, the first set of spheroids that underwent immunohistochemistry were stained for CD206 at a 1:100 dilution, but after imaging, it

was determined that 1:100 dilution was too high. Therefore, the two conditions stained for CD206 for this round of IHC (3 time consecutive injuries at 3 days post-injury and control with rosiglitazone treatment) are not appropriate for comparison to the rest of the data, and were removed for further analysis. The rest of the spheroids that were stained for CD206 were then stained at 1:200 dilution. The results for the 1:200 diluted CD206 staining is described below.

10 spheroids for the 4kRPM single injury conditions at 3 days, 5 days, and 7 days post-injury (DPI) and control were collected for CD206. The total mean intensities were calculated for each of these timepoints.

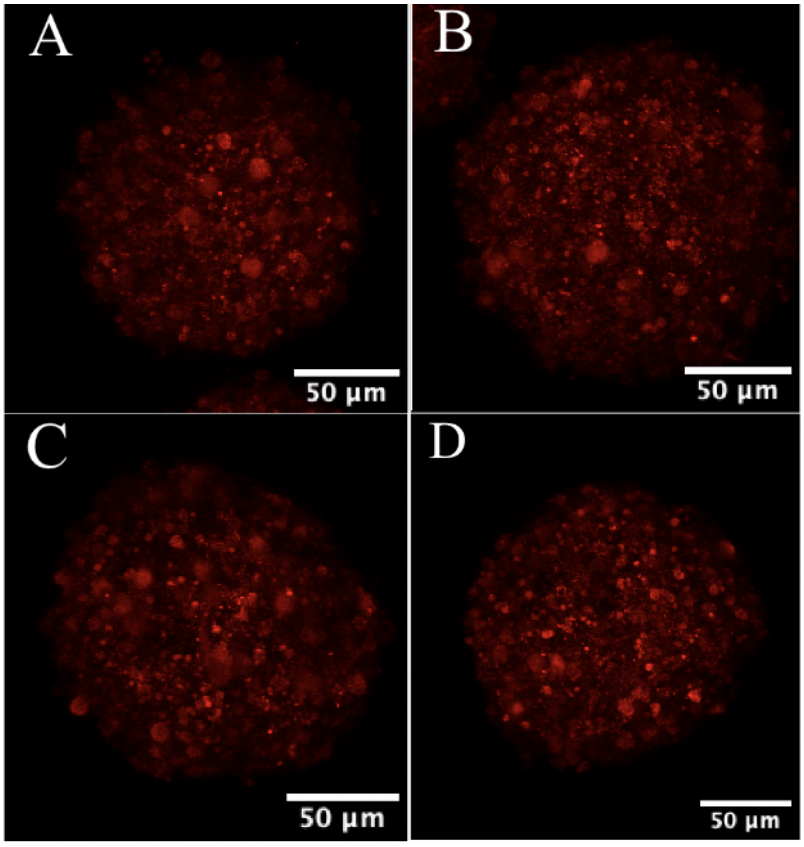

Figure 16: No clear differences in morphology or brightness between single-injury spheroids A) Control B) 4kRPMx1 3DPI C) 4kRPMx1 5DPI D) 4kRPMx1 7DPI

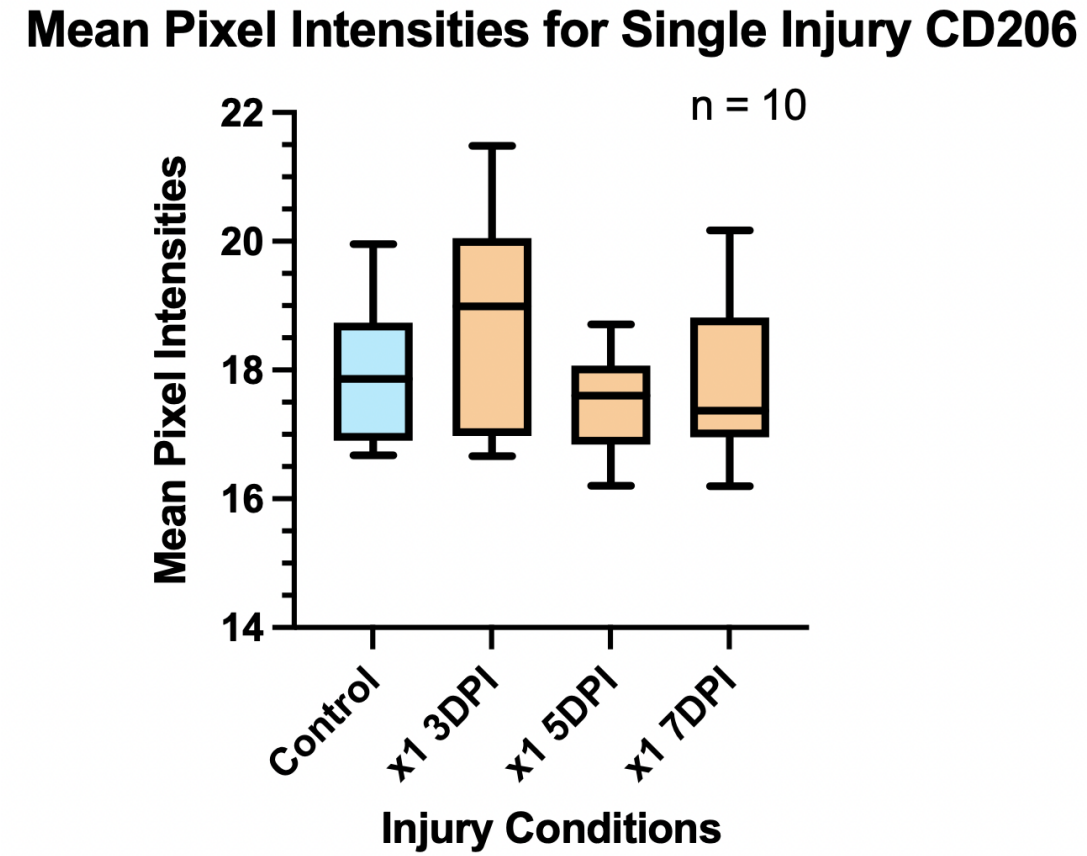

Figure 17: No significant differences between the total mean intensities for the single injury conditions. Box plot for the single injury conditions spheroids stained for CD206. Center lines of the box plot represent the median. The lower and upper whiskers represent the minimum and maximum values, and the box extends from the 25th to 75th percentiles of the datasets

Comparing the z-stack images between the conditions for the single-injury for CD206, there are no clear differences in morphology or brightness between the spheroids (Figure 16). After confirming that the data passed both the normality and variance tests, the Tukey test was run on each pair of the data set to test for significance. There were no significant differences in the total mean intensities of the CD206 expression across all single injury conditions and the control group. There is a trend in the median line, where the median mean pixel intensity peaks at 3 days post-injury, and then decreases at 5 days

post-injury and 7 days post-injury. Overall, there were no significant differences in CD206 expression in these injury conditions.

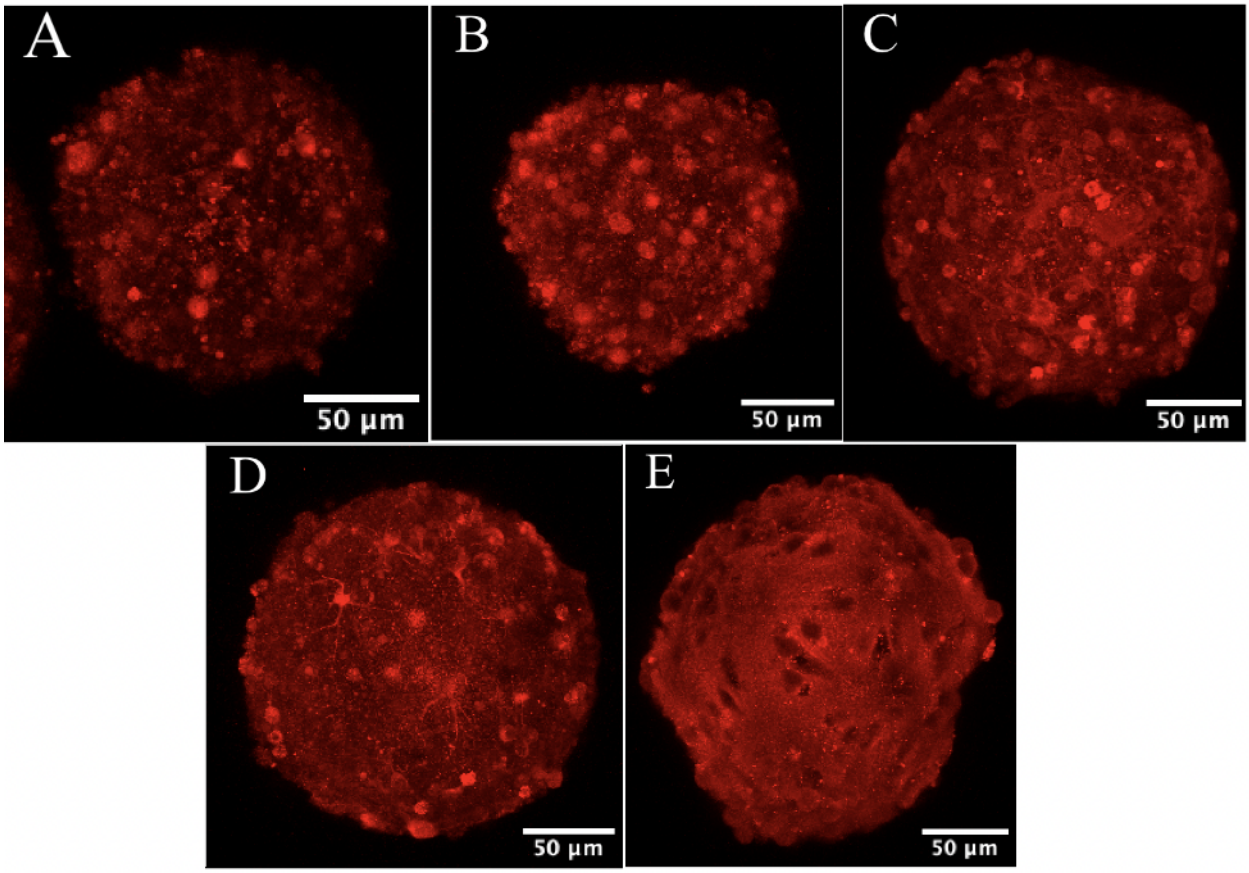

Figure 18: Clear changes in morphology at 3DPI onwards in repeated injury spheroids stained with CD206 Z-stack images of three times repeated injury conditions stained for CD206 A) Control B) 4kRPMx3 at 0H C) 4kRPMx3 24H D) 4kRPMx3 5DPI E) 4kRPMx3 7DPI

The spheroids were also injured three-times consecutively. The z-stack images for the three repeated injury conditions immediately after injury (0H), 24 hours post-injury, 5 days post-injury, and 7 days post-injury were compared. Within this repeated injury group, there is a clear change in morphology between the various time points after injury. The change in morphology is most noteworthy at 7 days post-injury, where the microglial cells are not as distinctive as the confocal images for the other spheroid conditions.

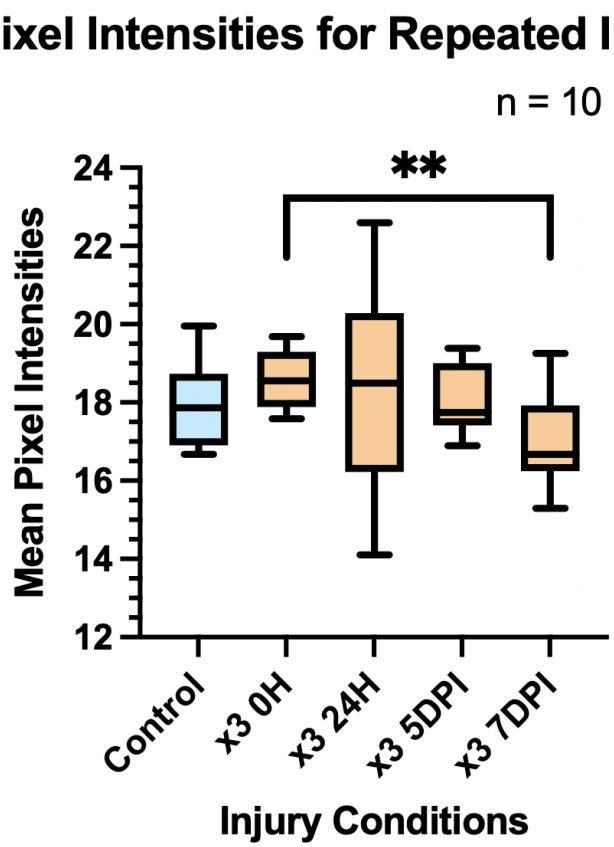

Figure 19: The total mean gray intensities for 0H and 7DPI were significantly different for the repeated injury conditions. Box plot for three repeated injury conditions. Center lines of the box plot represent the median. The lower and upper whiskers represent the minimum and maximum values, and the box extends from the 25th to 75th percentiles of the datasets

** $p < 0.01$

Statistical tests for the repeated injury conditions were conducted to test for significance. The repeated injury data was tested for normality and unequal variance, and passed the normality test but did not pass the equal variance test with a significance level of 0.05. Normality and unequal variances were tested for each pair of conditions that were compared, and if it passed, the ANOVA test was run to test for significance using a p-value of 0.05. This was the case for every comparison that did not involve the x3 24H group. If the pair of conditions passed the normality test but failed the unequal variance test, the

Welch's test was run and tested for significance using a Bonferroni adjusted value of 0.0125. This was the case for the comparisons of every pairing involving the x3 24H. The only comparison that showed a significant difference was repeated injury at 0H and 7 days post-injury, where the p-value was 0.0046 < 0.01.

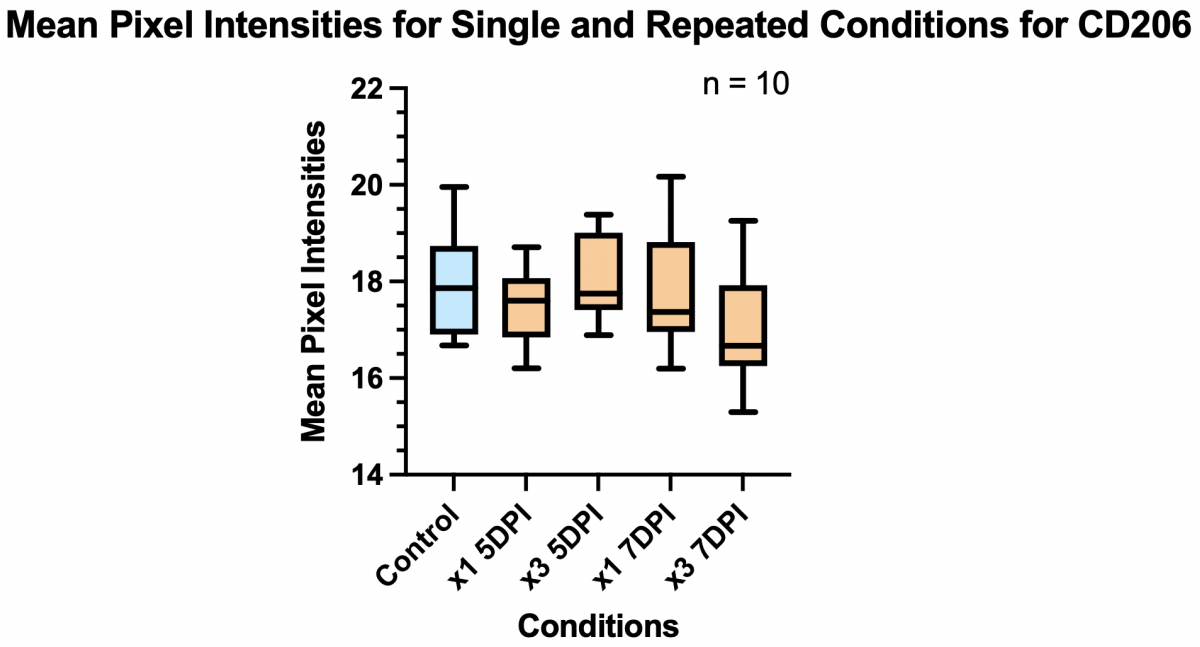

Figure 20: No significant differences between single and repeated injury conditions for total mean pixel intensities for CD206 Box plot for three repeated injury conditions. Center lines of the box plot represent the median. The lower and upper whiskers represent the minimum and maximum values, and the box extends from the 25th to 75th percentiles of the datasets

To compare the single and repeated conditions, only the conditions that matched the same time points were compared to each other, and to the control group. The data was tested for both normality and equal variance, and after confirming it passed both, the ANOVA test was run. The data was not statistically significant, indicating that there are no significant differences between the single and repeated injury conditions for the CD206 expression.

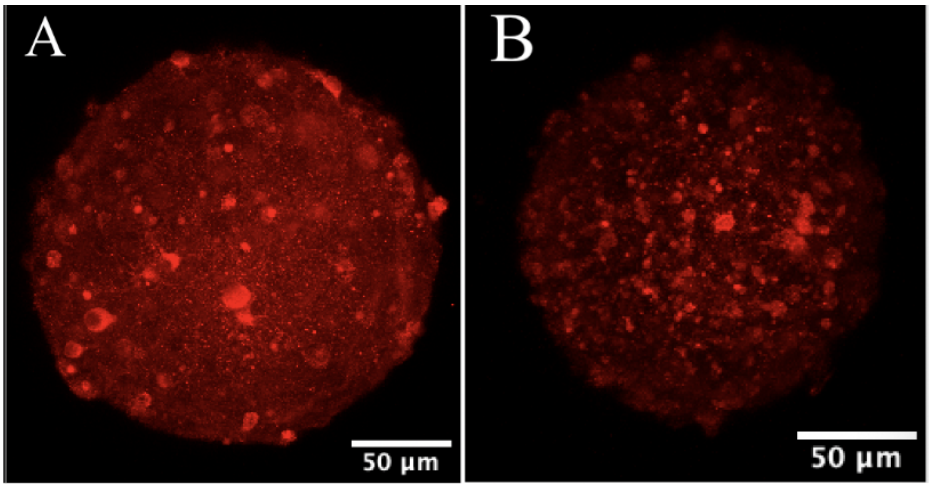

Figure 21: The morphology for rosiglitazone treated spheroids is more fragmented Z-stack images of injury conditions treated with and without rosiglitazone and stained for CD206 A) 4kRPMx3 5DPI B) 4kRPMx3 5DP ROSI

The spheroids were also treated with rosiglitazone and stained for CD206, to obtain a positive control for the data. Rosiglitazone is known to induce an M2-like state in microglia, meaning an increase in CD206 was expected (Peng et al., 2019). Comparing the morphologies with the control, rosiglitazone produced a slightly more fragmented appearance of CD206 staining, with a weaker background noise.

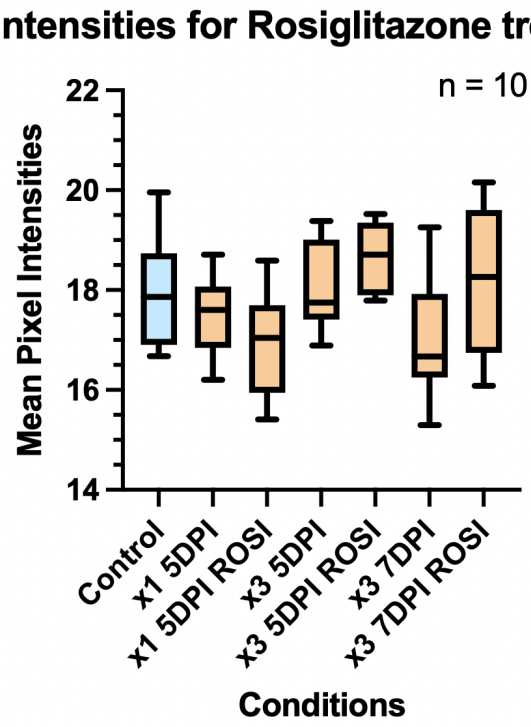

Figure 22: No significant differences in total mean pixel intensities with and without rosiglitazone treatment Box plot for three repeated injury conditions. Center lines of the box plot represent the median. The lower and upper whiskers represent the minimum and maximum values, and the box extends from the 25th to 75th percentiles of the datasets.

Statistical tests were then run on the total mean pixel intensities for comparison of treatment with and without rosiglitazone. The data was tested for normality and equal variance, and after confirming it passed, the ANOVA test was run for significance. There was no significant difference between the conditions treated with and without rosiglitazone.

Mean Pixel Intensities and Sphericity Measurements for P2Y12R

The next marker that was tested was P2Y12R, which is a marker known specifically for microglia. Because many neuroinflammatory markers are also expressed in macrophages, staining with

P2Y12 was an important method to distinguish the microglia from other cells (Jurga et al., 2020). It has also been shown to be highly expressed in its resting state, thus serving as a useful marker to identify resting microglia from activated microglia (Korzhevskii et al., 2021). The following datasets were stained for P2Y12R at 1:50 dilution, which was found to be the optimal dilution as seen from the 2D dilution tests.

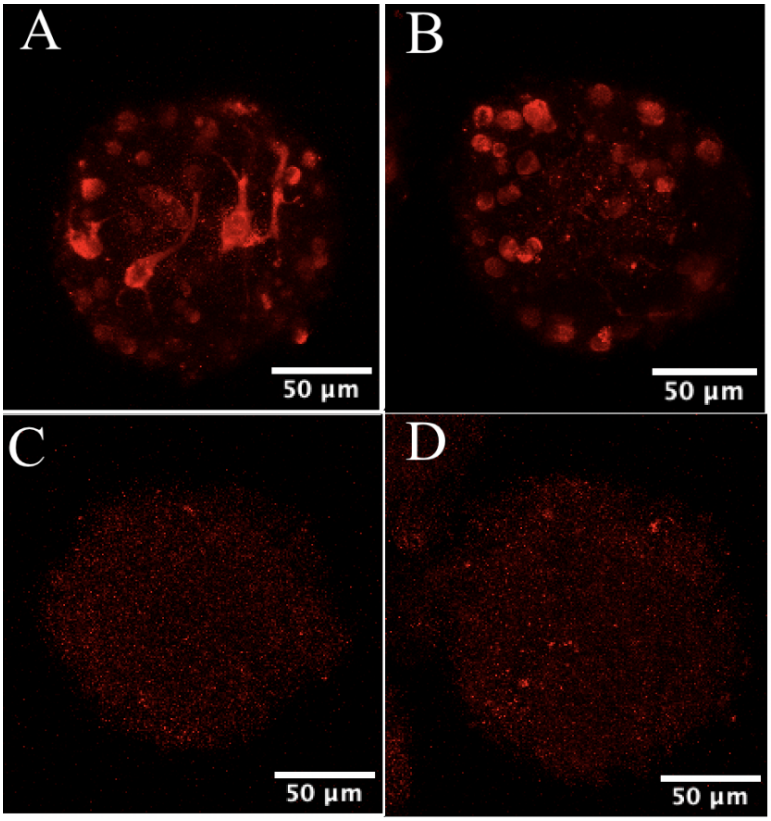

Figure 23: No P2Y12Ris detected at later time points after 3DPI Z-stack images of control and single injury conditions stained for P2Y12RA) Control B) 4kRPMx1 3DPI C) 4kRPMx1 5DPI D) 4kRPMx1 7DPI

P2Y12 was not detected at 5DPI or 7DPI, and was only detected in controls and at 3DPI for single injury conditions. Looking at the morphology, the microglia appear to be more rounded, which is known as an indication of activated microglia (Gómez Morillas et al., 2021).

A)

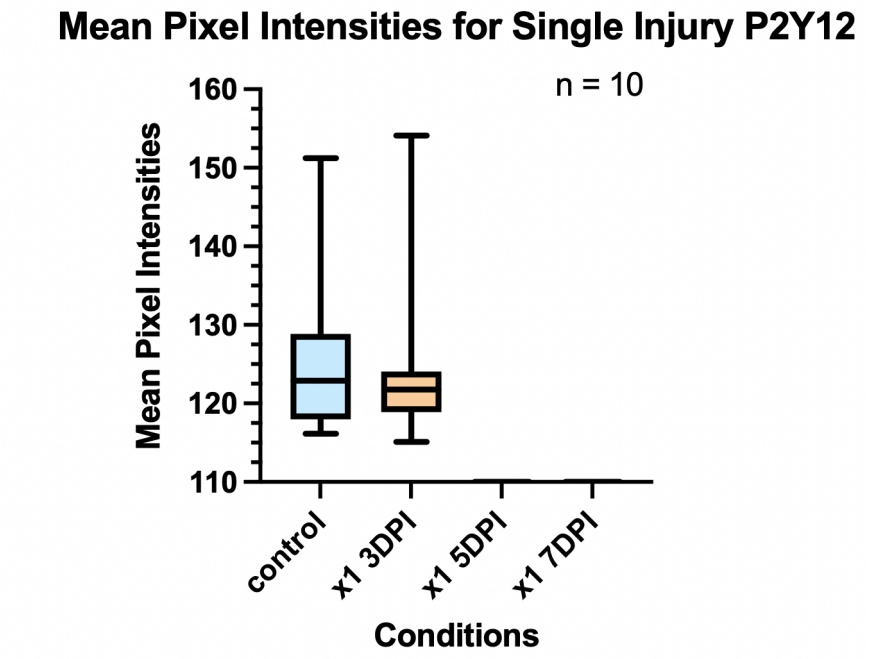

B)

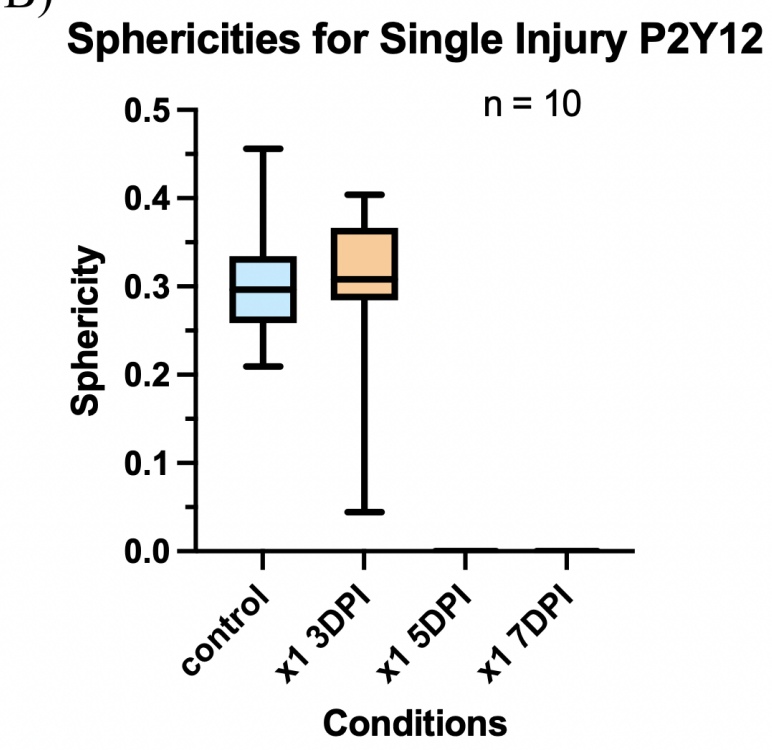

Figure 24: No significant difference in mean pixel intensities and sphericities between the control and 3DPI for single injury conditions A) Box plot for single injury conditions stained for P2Y12RB)

Box plot for sphericity measurements for single injury conditions for P2Y12R . Center lines of the box plot represent the median. The lower and upper whiskers represent the minimum and maximum values, and the box extends from the 25th to 75th percentiles of the datasets.

The mean pixel intensities for P2Y12R were collected for the single injury conditions, but there was no P2Y12R detected in the spheroids at 5 days and 7 days post-injury. The mean pixel intensities for single injury at 3 days post-injury and the control were tested for normality and equal variance. The data failed the normality test but passed the equal variance test. The Wilcoxon/Kruskal Wallis Test was performed, and revealed that the data was not significant, indicating that there is no significant difference between the control and P2Y12R expression at 3 days post-injury. Comparing the medians for both conditions also confirms that there is not a large difference between the sphericity for the two conditions.

The sphericity measurements for single injury conditions stained for P2Y12R were collected and analyzed, in order to characterize the morphology of the microglia. The Wilcoxon/Kruskal Wallis test was performed after it failed the normality and equal variance tests. There was no significant difference found between the sphericities for control and 3 days post-injury for single injury.

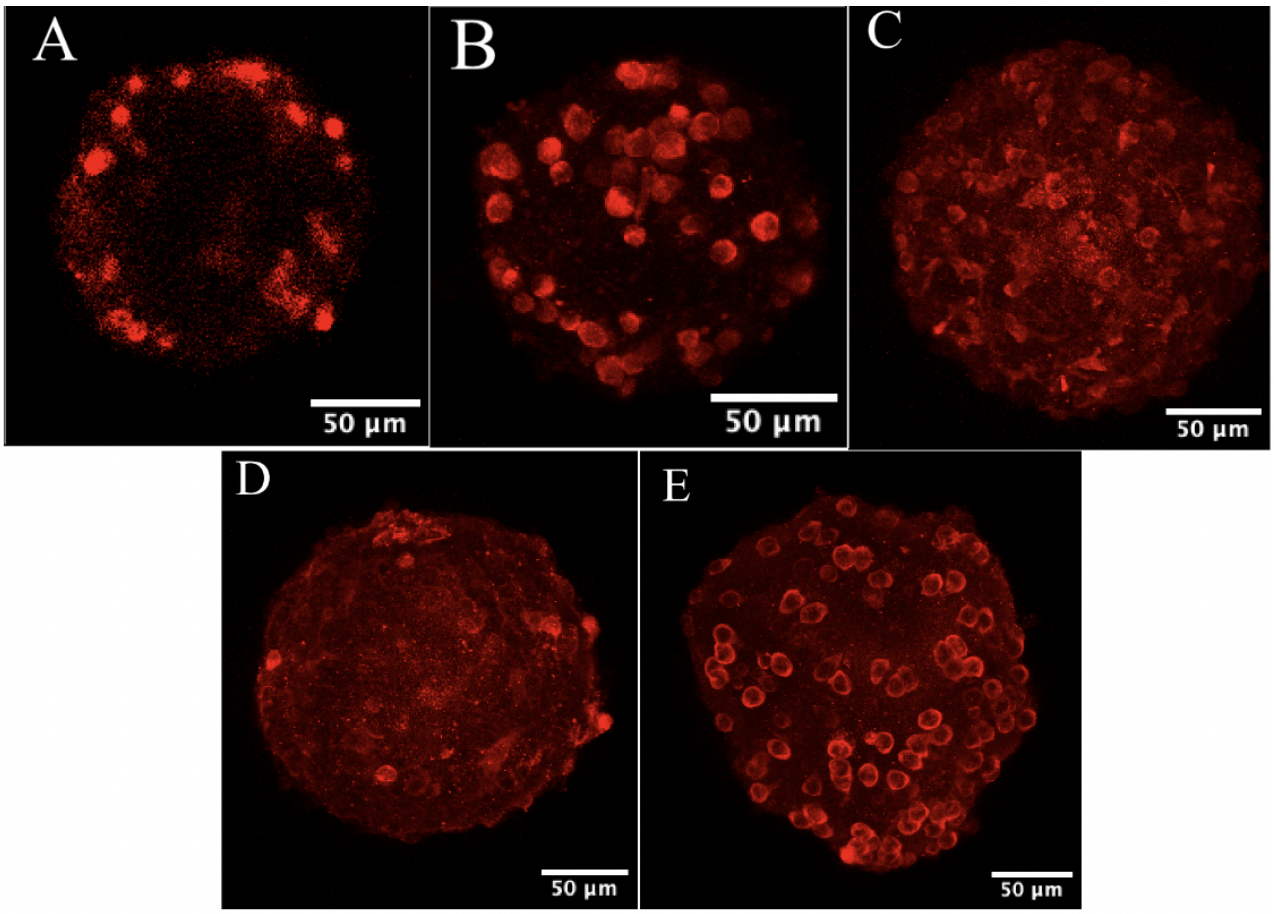

Figure 25: For repeated injury conditions, there is a clear change in morphology of microglia staining after 0H. Representative z-stack images of control and repeated injury conditions stained for P2Y12RA) Control B) 4kRPMx3 0H C) 4kRPMx3 24H D) 4kRPMx3 5DPI E) 4kRPMx3 7DPI

Looking at Figure 25, a morphological transformation was seen between 0H and 24H post-injury. The microglial cells are no longer clearly distinguishable, and appear to have a more irregular appearance with darker centers. This is most evident at 7DPI, where the microglial cells appear darker in the center of the cells.

A)

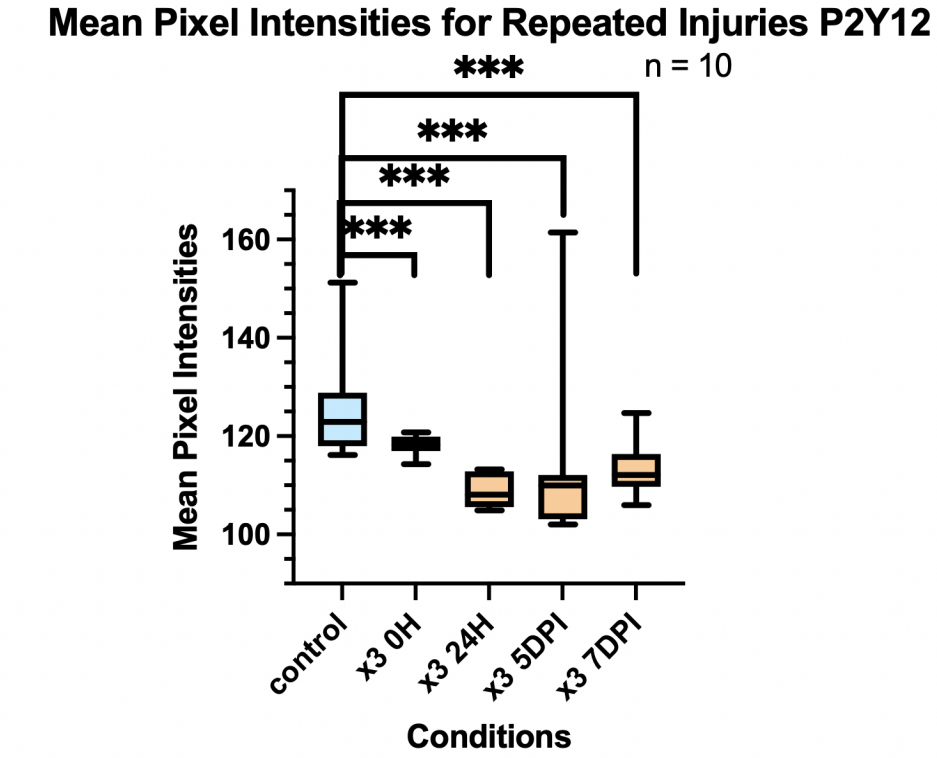
Mean Pixel Intensities for Repeated Injuries P2Y12
***
n = 10
***
***
***
Mean Pixel Intensities
160
140
120
100
control
x3 0H
x3 24H
x3 5DPI
x3 7DPI
Conditions

B)

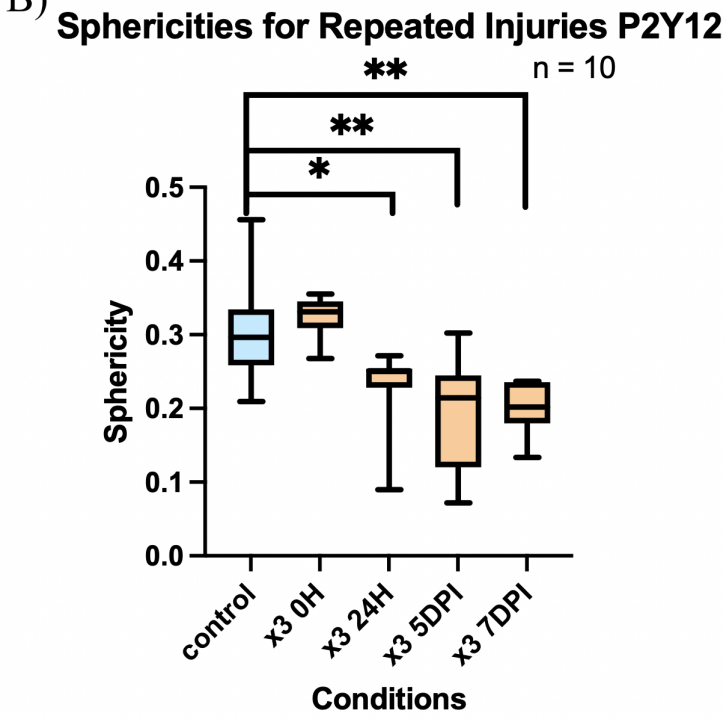
Sphericities for Repeated Injuries P2Y12
**
n = 10
**
*
Sphericity
0.5
0.4
0.3
0.2
0.1
0.0
control
x3 0H
x3 24H
x3 5DPI
x3 7DPI
Conditions

Figure 26: Significant differences for total mean pixel intensities and sphericities between control and most of the other conditions. A) Box plot for mean pixel intensities for repeated injuries stained for P2Y12RB) Box plot for sphericity measurements for repeated injury conditions for P2Y12R . Center lines of the box plot represent the median. The lower and upper whiskers represent the minimum and maximum values, and the box extends from the 25th to 75th percentiles of the datasets.

* $p<0.05$ ** $p<0.01$

The mean pixel intensities for three repeated injuries stained for P2Y12R were collected and normality and equal variance tests were run on the data. It failed both normality and equal variance, so the data was tested for a median test for comparisons between the control group and each of the injury conditions. At all time points, there was a significant difference in the mean pixel intensities for P2Y12R compared to the control.

The sphericity measurements for three repeated injuries were collected and statistical significance was calculated for the data. The data failed both the normality and equal variance tests. The median test was run on the data, and found significant differences between control and 24H, 5 days, and 7 days post-injury. There was no significant difference found between the sphericity measurements for control and 0H. This is in accordance with what is seen in the morphological analysis, as described earlier.

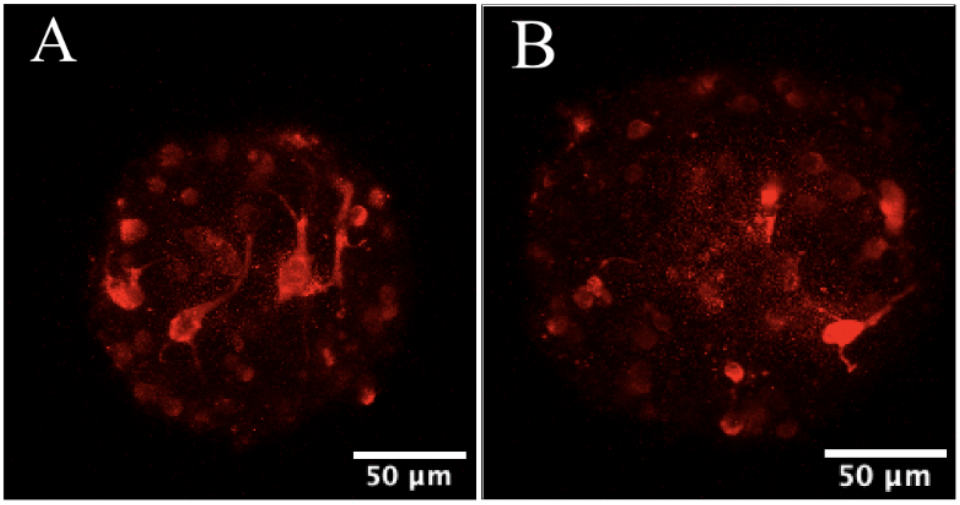

Figure 27: No change in morphology between the rosiglitazone treated spheroid for 4kRPMx1 5DPI and the control. No P2Y12R detected for rosiglitazone treated spheroids for repeated injury conditions Representative z-stack images of control and rosiglitazone treated spheroids A) Control B) 4kRPMx1 5DPI treated with Rosiglitazone

Similar to in CD206 staining, there is no clear change in morphology between the rosiglitazone treated spheroid and the control for P2Y12R .

A)

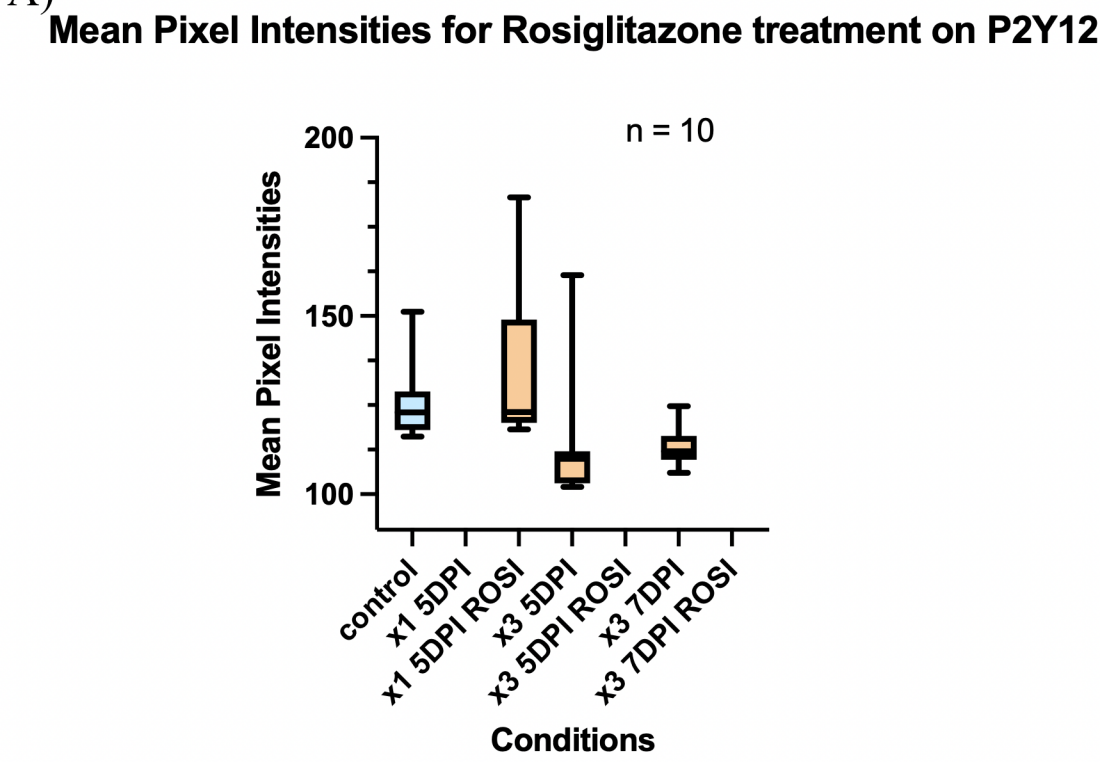

B)

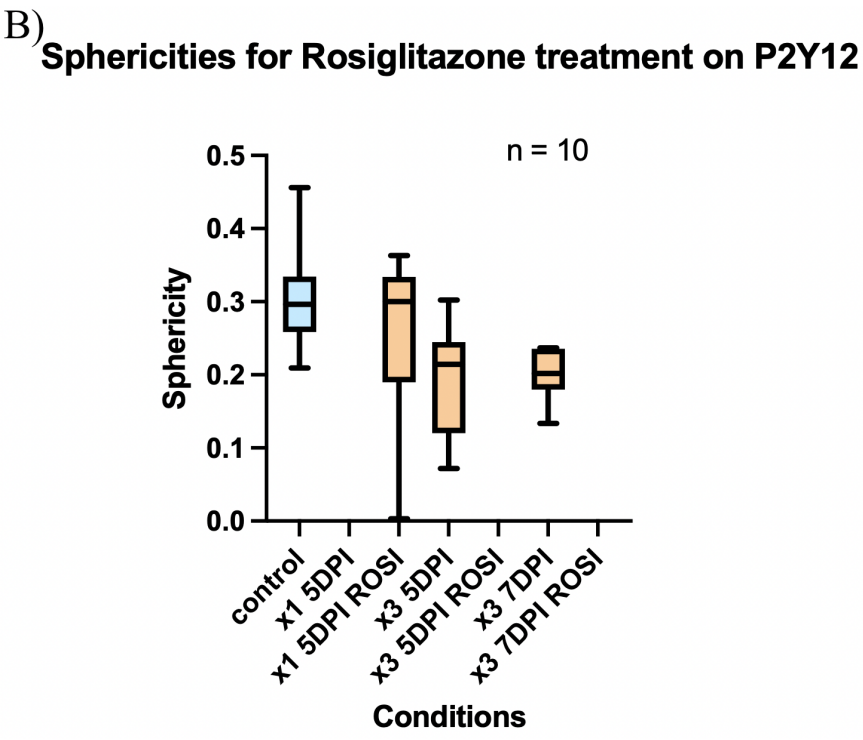

Figure 28: No significant differences in total mean pixel intensities or sphericities for rosiglitazone treated spheroids A) Box plot for three repeated injury conditions B) Box plot for sphericity

measurements for repeated injury conditions for P2Y12R . Center lines of the box plot represent the median. The lower and upper whiskers represent the minimum and maximum values, and the box extends from the 25th to 75th percentiles of the datasets.

The spheroids treated with rosiglitazone were also stained with P2Y12R and compared with the non-treated spheroid groups at the same time points. There was no P2Y12R detected at single injury 5 days post-injury, three times repeated injury 5 days and 7 days post-injury both treated with rosiglitazone. There was no significant difference between the control group and single injury 5 days post-injury treated with rosiglitazone, when using the median test after both normality and variance failed.

After checking that the data failed both normality and equal variance tests, the median test revealed that there was no significant difference between the sphericity measurements for control and the single injury 5 days post-injury treated with rosiglitazone.

Discussion

Marker (dilution)	**3D Conditions Tested**	**Results**
CD86 (1:100)	Control, 24H and 3 day exposure to LPS, 4kRPMx1 7DPI, 4kRPMx3 5DPI and 7DPI	No CD86 detected
CD16 (1:50)	Control, 3day LPS exposure, 4kRPMx3 3DPI	No CD16 detected
CD206 (1:200)	Single injury conditions: Control, 3DPI, 5DPI, 7DPI	No significant difference in mean pixel intensities
CD206 (1:200)	3x Repeated injury conditions:	Significant difference in total

	Control, 0H, 24H, 5DPI, 7DPI	mean intensities between 0H and 7DPI, but no other significant difference
CD206 (1:200)	Rosiglitazone treated spheroids: X1 5DPI, x3 5DPI, x3 7DPI	No significant difference in mean pixel intensities
P2Y12R(1:50)	Single injury conditions: Control, 3DPI, 5DPI, 7DPI	No P2Y12 detected at 5DPI and 7DPI, no significant difference found between control and 3DPI for mean pixel intensities or sphericities
P2Y12R (1:50)	Repeated injury conditions: Control, 0H, 24H, 5DPI, 7DPI	Significant differences found between control and at all time points for mean pixel intensities; significant differences for sphericities between control and 24H, 5DPI, 7DPI
P2Y12R(1:50)	Rosiglitazone treated spheroids: x1 5DPI, x3 5DPI, x3 7DPI	No significant differences found in mean pixel intensities and sphericities

Table 7: Significant differences found in repeated injury conditions for CD206 and for repeated injury conditions for P2Y12R. This is a summary table of all the 3D conditions tested and markers that were used to stain the spheroids.

This study looked at neuroinflammatory markers in single and repeated mTBI using a rat cortical spheroid model. The injury model consisted of single or three-times repeated centrifugal injury, and neuroinflammation was assessed at the following time points: 0H, 24H, 3 days post-injury, 5 days post-injury, and 7 days post-injury. The spheroids were stained for the following markers: CD86, CD16, CD206, P2Y12R , and Iba1. As a positive control, the spheroids were stimulated with LPS, as it is an established *in vitro* model for neuroinflammation in TBI. This is because similar to exposure to TBI, stimulation by LPS upregulates major proinflammatory mediators such as TNF-α and IL-1β in microglia in *in-vivo* mice and rat cortices, and have proven to increase expression of CD86 (Kumar et al., 2017; Ponomarenko et al., 2021). Moreover, LPS-treated cells showed altered microglial morphology, changing from a rounded and fusiform shape to a more spread out and increased size, indicating their activation (Ponomarenko et al., 2021). It must be noted here that while blood brain barrier (BBB) disruption plays an important role in neuroinflammation after TBI with the influx of peripheral immune cells, the spheroid model used in this study does not have a BBB so the neuroinflammation is only caused by resident cells (microglia and astrocytes).

CD86 and CD16 Expression

CD86 was chosen as a marker because it is one of the most well-studied markers of neuroinflammation in the brain for M1-like microglia (Jurga et al., 2020; Peruzzaro et al., 2019). Several TBI studies have seen a significant increase in CD86 expression after TBI. For example, Zhu et al. found that at 4 days post-TBI, there was a significant increase in the expression of CD86 in the rat cortical tissue *in-vivo* (Zhu et al., 2020). Peruzzaro et al. found a significant increase in CD86 expression *in-vivo* at 36 hours post-injury in rats (Peruzzaro et al., 2019). Additionally, Ponomarenko et al. examined CD86 expression for both mTBI via weight-drop model and LPS exposure. CD86 expression was increased at 7 days post-TBI in the rat cortex and also increased in the murine microglial cell line SIM-A9 *in-vitro* after 24H exposure to LPS (Ponomarenko et al., 2021). However, in this current study, CD86 was not detected

via immunofluorescence in any of the conditions and time points that were tested, both in 2D testing and in spheroids. Thus, another common M1-like marker for microglia, CD16, was also tested.

CD16 expression via immunofluorescence has been shown to be increased in the *in-vivo* rat and mice cortex at 3 days after TBI, and remains elevated at 7 and 21 days post-TBI (Harvey et al., 2015; Wang et al., 2013; WenLiang et al., 2018; Zhao et al., 2020). Wang et al. also found that CD16 expression peaked at 3 days post-TBI in the rat cortex. These results were confirmed using real time RT-PCR findings (Wang et al., 2013; WenLiang et al., 2018). Gao et al. also found a significant increase in CD16 and a slight increase of CD86 in the *in-vivo* ipsilateral mouse brain at 7 days post-TBI via Western blotting (Gao et al., 2016). However, CD16 was also not detected in any of the conditions in this study. There are several reasons that may account for the lack of detection of CD86 and CD16.

First, there is a possibility that the antibodies that were tested were not suitable for immunohistochemistry. The main application for the CD86 was flow cytometry and for CD16 was recommended for IHC-P. It must be noted that most TBI papers looking at neuroinflammatory markers measure gene expression, which has a much more robust expression compared to measuring fluorescence expression. Secondly, the antibodies may not be optimal for the immunohistochemistry protocol used. For example, the incubation time may be too short or the type of IHC (formalin fixed, paraffin-embedded, fresh frozen, etc) may not have been optimal (*IHC Troubleshooting | Abcam*, n.d.). Finally, the expression of CD86 has shown a varied response in prior TBI studies. While CD86 expression was increased in various mTBI studies mentioned above, some studies also found that the CD86 expressions were irregular. CD86 expression was evident at much later time points or had inconsistent expression in other studies. Jin et al. found that CD86 is only highly expressed after a longer time period of 28 days post-injury via controlled cortical impact (CCI) compared to 7 days or 14 days post-injury in *in vivo* mice (Jin et al., 2012). Furman et al. found CD86 expression was inconsistent at 24H and had an overall low expression of CD86 on activated microglia in *in-vivo* rats after CCI (Toledano Furman et al., 2020).

Furthermore, CD86 and CD16 expression may only be present in low abundance, especially in a rat neonatal cortex. Thus, an amplification process may be needed to bring the molecules to detectable levels.

P2Y12R expression

The purinergic system plays a vital role in the CNS, where both purines and pyrimidines serve as extracellular molecules to mediate inter-glial and neuron-to-gia interactions. Microglia express a range of ionotropic P2X and metabotropic P2Y receptors. P2Y12R, which is also known to be a microglial specific marker, has been shown to have high expression in its surveillant state, with a ramified morphology (Jurga et al., 2020; Kumar et al., 2016). After a brain injury occurs, microglia transform into a process-extending phenotype and increase their motilities, which allows them to extrude processes to the site of injury (Koizumi et al., 2013). Haynes et al. found that this process extension is dependent on microglial P2Y12 receptors recognizing the presence of ATP released from damaged cells in the brain (Charolidi et al., 2015; Haynes et al., 2006). Then, P2Y12R is downregulated and ARA2A is upregulated, leading to the retraction of the microglial processes. The microglia then transform into an amoeboid morphology and start phagocytosis, pinocytosis, or secretory activities depending on the purinergic receptor that is involved (Gómez Morillas et al., 2021).Thus, for this study, due to the changing shape of microglia when activated, sphericity was an output that was calculated in addition to the intensity of the signal for P2Y12R. Looking at the z-stack images of P2Y12R for single injury conditions, the spheroids at 3DPI appear to have a rounder shape compared to the control, where some branches are visible. However, there was no statistical difference in the sphericities between the control and the 3DPI spheroids. There is a clearer distinction in the morphology between time points in three consecutive repeated injury conditions for P2Y12R, and statistical calculations have confirmed that there is a statistically significant difference. For the repeated conditions, immediately after injury microglia appear to be more round compared to the control, with some branching seen at 24H. At 5DPI, there seems to be the greatest amount of branching, appearing to have a more ramified shape. It is interesting to see that

then at 7DPI, the microglia again assume an amoeboid shape but appears more hollow-like compared to at 0H. This is in contrast to the previous literature, where it's been described that in TBI microglia undergo a morphological change from a ramified state to the retraction of the fine processes, which lead to the amoeboid shape with thick bundles surrounding it, characteristic of an activated state (Heindl et al., 2018; Kumar et al., 2017). Fernandez-Arjona et al. break down the microglia morphology into four forms: (i) ramified resting/inactive ii) hypertrophied iii) bushy and iv) unramified reactive/amoeboid microglia, so these changing morphology may reflect this variety in morphology (Fernández-Arjona et al., 2017). These states can also include the transitional states of microglia from a resting state to reactive to activated states (Karperien et al., 2011). Fernandez-Arjona et al. also noted that brain location played a factor in the morphology of microglia as well. For example, surveillant microglia in some brain areas showed similar morphological features as activated microglia in other brain areas in *in vivo* male Wistar rats, thus hinting that brain location may play a role in morphological phenotype (Fernández-Arjona et al., 2017). Furthermore, Talib et al. has also found that in more severe TBI models, microglia express both pro and anti-inflammatory phenotypes at early time points post-TBI, and the up-regulatiion of M2 phenotype was replaced with a "Mtransitional" phenotype that consists of both M1 and M2 markers at 7 days post-injury in CCI models of mice(Taib et al., 2017; Witcher et al., 2015). This "Mtransitional" phenotype may be what is seen here at 7DPI.

The P2Y12R expression was not detected at 5 days and 7 days after single injury, and yet was detected at all timepoints in repeated injury conditions. P2Y12R was expressed in all controls, which is in line with prior studies stating that P2Y12R expression is highly detected in its resting state (Toledano Furman et al., 2020). Moore et al. describes that P2Y12R expression decreases when the microglia are in an M1-state, but again increases expression when activated to its M2 state seen in *in vitro* human brain tissue (Koizumi et al., 2013; Moore et al., 2015). Because M2 expression has been shown to occur early in the injury progression and has a transient expression, this may explain why there is expression at 3DPI but not at 5DPI and 7DPI. However, there are also differences seen in expression in single injury

compared to that of repeated injury. One possible explanation is that the single injury is insufficient to produce a significant change in microglia, especially with the 3 days of recovery time. Repeated TBI models have indicated that repeated brain injuries result in a much greater and prolonged microgliosis response compared to single injury (Bolton & Saatman, 2014; Bolton-Hall et al., 2019). For future studies, more time points such as 0H and 24H for single injury conditions should also be examined to compare the data between single and repeated injury conditions.

Rosiglitazone treatment also did not produce a significant difference in both intensities or sphericities. This is as expected, as rosiglitazone is known to induce M2-like state in microglia, and so these results are in accordance with Moore et al., where they describe that P2Y12R is expressed in a resting state and in an M2 state (Moore et al., 2015). However, rosiglitazone treatment resulted in no detection of P2Y12R for repeated injury conditions at 5DPI and 7DPI, which may suggest that at more severe injuries, there is a lower expression of M2-microglia and an increase in M1-microglia. However, this was unable to be confirmed in this current study due to the lack of M1-marker detection.

CD206 Expression

CD206 was examined as an M2 microglia marker for single and repeated injuries, as it is a common marker that has been studied in TBI papers. Due to issues with the 2D controls, there was no test control conducted for CD206 to find the optimal antibody dilution. The results in this paper only analyzed the 1:200 dilution for CD206, but reflecting on the Tiff files for CD206, there is still some background with 1:200 dilution. Thus, a higher dilution of 1:300 or 1:500 may be more optimal for this spheroid model. Other papers using the same biomarker have tested for higher dilutions ranging from 1:300 to 1:1000 (Borgatti et al., 2021; Galarraga-Vinueza et al., 2021; Wu et al., 2021; Yang et al., 2021).

CD206 is expressed in control tissue but with low expression and has been shown to increase after TBI as seen in human brain tissue samples (Bohnert et al., 2020). Relative intensity for CD206 marker was increased in TBI at 3 days in a Feeny DM TBI model of rats (Chen et al., 2018) and Wang et

al. found that CD206 expression was significantly greater in the ipsilateral cortex of mice after TBI compared to controls, and increased at 3 days post-injury, peaked on day 5, and then decreased to baseline on day 14. At the same time, they found that the CD206 expression peaked on day 3 in the ipsilateral corpus callosum area, and only slightly increased expression compared to controls in the contralateral corpus callosum. Thus, the expression of CD206 varies depending on the brain region (Wang et al., 2013). Looking at Figure 17 and 19, there is a slight increase in the medians for CD206 intensities at earlier time points shortly after TBI, before it decreases back down. This may reflect the transient state of M2 microglia shortly after TBI injury, before shifting to M1 (Wang et al., 2013). However, compared to controls, there was no significant increase in CD206 expression for all injuries. It was unexpected to see that there were no significant differences between the single injury conditions and the repeated injury conditions, as Aungst et al. found that repeated mTBI causes a significantly increased neuroinflammatory response compared to that of a single mTBI (Aungst et al., 2014). However, this is in accordance with Bohnert et al., which found that there was no significant CD206 expression in all TBI cases compared to controls in the cortex, but did find a significant difference in expression of CD206 in the white matter and cerebellum. Thus, there is a possibility that while CD206 expression isn't significant in the cortex, it may show increased expression when looking at other brain regions (Bohnert et al., 2020).

Rosiglitazone treatment also did not have a significant difference on the expression of CD206. This is not as expected, as prior studies have shown that rosiglitazone treatment increases CD206 expression. Rosiglitazone treatment has been shown to induce a significant increase of CD206 expression when compared to TBI or other forms of brain injury like status epilepticus, but is not statistically significant when compared to controls as seen in TBI models of mice (Li et al., 2019; Peng et al., 2019).

While, the mechanism of action for microglial activation in neuroinflammation still has large gaps of knowledge, Wu et al. has proposed that myeloid-epithelial-reproductive tyrosine kinase (Mer), a member of the Tryo-Axl-Mer (TAM) family may play an important role in regulating the M1/M2 polarization for microglia and macrophages in neuroinflammation. They demonstrated that the

upregulation of Mer mediates the activation of the STAT1/SOCS signaling pathway implicated in providing neuroprotective effects in a controlled cortical impact model in mice, by increasing M2-like polarization. However, they also note that due to the mounting evidence that there are cells that dually express both M1 and M2 phenotypes, the binary M1/M2 polarization paradigm may not accurately represent the neuroinflammatory profiles of microglia after TBI. Thus, further research on various TBI neuro inflammatory markers is necessary to better understand the neuroinflammatory pathway after TBI (Wu et al., 2021).

Limitations

There are several limitations to this study that must be addressed. First, a much larger n group is required to confirm the validity of this data because a sample size of n=10 per condition is too small to accurately test for statistical significance. Additionally, there was only one control group per biomarker. In order to accurately make comparisons between the experimental groups and the control groups, there must be control groups per time point that was measured. For this study that would mean having a control group fixed at 0H, 24H, 3DPI, 5DPI, and 7DPI. This is important to ensure that the spheroids are at the same DIV and do not differ in size. On a similar note, there were issues with the dissections and so the sizes of the spheroids were not uniform and there was a lack of 2D controls. As stated in the Results section, there were no 2D controls to test antibody dilutions for CD16 and CD206, which hindered the ability to test for the optimal dilution before the injuries were conducted. Furthermore, for the analysis, the exact same threshold and size were chosen per biomarker for 3D Object Counter analysis. This was done to ensure that there is no variability in analysis. One caveat is that the same threshold and size did not necessarily capture all of the microglia for every condition, and thus some microglia may have been miscounted.

Future Directions

For future directions, there are several variables in this study that could be examined. First, another biomarker for M1 microglia such as CD11 or CD45 should be tested in order to examine M1 microglia behavior in single and repeated mTBI for this spheroid model (Toledano Furman et al., 2020). Testing for a greater range of antibody dilutions on 2D test controls would also be beneficial to optimize the antibody concentration for this spheroid model.

Another possibility would be to alter the rosiglitazone concentration that the spheroids were treated with. In this study, the concentration of rosiglitazone was 1 μM, but several other papers have tested for rosiglitazone concentrations ranging from 0.1μM to 10 mM (Gogola et al., 2020; Ren et al., 2020). Similarly, the rosiglitazone administration time could also be altered. There are several papers that treated cells with rosiglitazone with longer time periods like 1 or 2 weeks (Kim et al., 2020; Ren et al., 2020). The timing of the administration also ranged, where Wen et al. treated mice with rosiglitazone 15 minutes before the brain injury, Yi et al. conducted rosiglitazone treatment at 5 minutes, 6 hours and 24 hours after injury, and Luo et al. conducted rosiglitazone treatment both before and after injury(Luo et al., 2006; Wen et al., 2018; Yi et al., 2008).

Likewise, the LPS treatment is also a variable that could be adjusted. The concentration of LPS, the exposure time, and the fixing time point after exposure are all factors that should be considered for future experiments.

Referencing last year's senior thesis, looking at various inter-injury intervals is another variable that is interesting to study. Researchers have reported that a 24-hour inter-injury interval between injuries simulates real-life scenarios of at-risk populations like athletes or military personnel (Nichols et al., 2016). Thus, repeating this current study with 24-hour inter-injury intervals is a possible model that can be studied in the future.

Conclusion

Neuroinflammation is one of the major processes that occur in TBI, and yet there is still a large gap in understanding the neuroinflammatory pathway. This study establishes a spheroid model that examines both single and repeated mTBI injuries and the inflammatory pathway that proceeds by testing for neuroinflammatory markers for microglia. Neuroinflammation has been associated with higher susceptibility to depression and anxiety, as well as other neurodegenerative processes (Brites & Fernandes, 2015; Chiu et al., 2016). Promoting the phenotypic transformation of microglia to a more neuroprotective state, while reducing neurotoxic effects, will be key to developing therapeutic applications for TBI (Harvey et al., 2015). Thus, more research needs to be conducted to gain a greater understanding of neuroinflammation in the brain.

References

3D Objects Counter. (2009, November 12). ImageJ Wiki. https://imagej.github.io/plugins/3d-objects-counter

Aungst, S. L., Kabadi, S. V., Thompson, S. M., Stoica, B. A., & Faden, A. I. (2014). Repeated mild traumatic brain injury causes chronic neuroinflammation, changes in hippocampal synaptic plasticity, and associated cognitive deficits. *Journal of Cerebral Blood Flow & Metabolism*, *34*(7), 1223–1232. https://doi.org/10.1038/jcbfm.2014.75

Bohnert, S., Seiffert, A., Trella, S., Bohnert, M., Distel, L., Ondruschka, B., & Monoranu, C.-M. (2020). TMEM119 as a specific marker of microglia reaction in traumatic brain injury in postmortem examination. *International Journal of Legal Medicine*, *134*(6), 2167–2176. https://doi.org/10.1007/s00414-020-02384-z

Bolton, A. N., & Saatman, K. E. (2014). Regional Neurodegeneration and Gliosis Are Amplified by Mild Traumatic Brain Injury Repeated at 24-Hour Intervals. *Journal of Neuropathology and Experimental Neurology*, *73*(10), 933–947. https://doi.org/10.1097/NEN.0000000000000115

Bolton-Hall, A. N., Hubbard, W. B., & Saatman, K. E. (2019). Experimental Designs for Repeated Mild Traumatic Brain Injury: Challenges and Considerations. *Journal of Neurotrauma*, *36*(8), 1203–1221. https://doi.org/10.1089/neu.2018.6096

Borgonetti, V., Sanna, M. D., Lucarini, L., & Galeotti, N. (2021). Targeting the RNA-Binding Protein HuR Alleviates Neuroinflammation in Experimental Autoimmune Encephalomyelitis: Potential Therapy for Multiple Sclerosis. *Neurotherapeutics*, *18*(1), 412–429. https://doi.org/10.1007/s13311-020-00958-8

Brites, D., & Fernandes, A. (2015). Neuroinflammation and Depression: Microglia Activation, Extracellular Microvesicles and microRNA Dysregulation. *Frontiers in Cellular Neuroscience*, *9*. https://www.frontiersin.org/article/10.3389/fncel.2015.00476

Capizzi, A., Woo, J., & Verduzco-Gutierrez, M. (2020). Traumatic Brain Injury: An Overview of Epidemiology, Pathophysiology, and Medical Management. *Medical Clinics of North America*, *104*(2), 213–238. https://doi.org/10.1016/j.mcna.2019.11.001

Charolidi, N., Schilling, T., & Eder, C. (2015). Microglial Kv1.3 Channels and P2Y12 Receptors Differentially Regulate Cytokine and Chemokine Release from Brain Slices of Young Adult and Aged Mice. *PLOS ONE*, *10*(5), e0128463. https://doi.org/10.1371/journal.pone.0128463

Chen, X., Chen, C., Fan, S., Wu, S., Yang, F., Fang, Z., Fu, H., & Li, Y. (2018). Omega-3 polyunsaturated fatty acid attenuates the inflammatory response by modulating microglia polarization through SIRT1-mediated deacetylation of the HMGB1/NF-κB pathway following experimental traumatic brain injury. *Journal of Neuroinflammation*, *15*(1), 116. https://doi.org/10.1186/s12974-018-1151-3

Chiu, C.-C., Liao, Y.-E., Yang, L.-Y., Wang, J.-Y., Tweedie, D., Karnati, H. K., Greig, N. H., & Wang, J.-Y. (2016). Neuroinflammation in animal models of traumatic brain injury. *Journal of Neuroscience Methods*, *272*, 38–49. https://doi.org/10.1016/j.jneumeth.2016.06.018

Cole, W. R., & Bailie, J. M. (2016). Neurocognitive and Psychiatric Symptoms following Mild Traumatic Brain Injury. In D. Laskowitz & G. Grant (Eds.), *Translational Research in Traumatic Brain Injury*. CRC Press/Taylor and Francis Group. http://www.ncbi.nlm.nih.gov/books/NBK326715/

Corps, K. N., Roth, T. L., & McGavern, D. B. (2015). Inflammation and Neuroprotection in Traumatic Brain Injury. *JAMA Neurology*, *72*(3), 355–362. https://doi.org/10.1001/jamaneurol.2014.3558

Dean, J. M., Wang, X., Kaindl, A. M., Gressens, P., Fleiss, B., Hagberg, H., & Mallard, C. (2010). Microglial MyD88 signaling regulates acute neuronal toxicity of LPS-stimulated microglia in vitro. *Brain, Behavior, and Immunity*, *24*(5), 776–783. https://doi.org/10.1016/j.bbi.2009.10.018

Di Pietro, V., Ragusa, M., Davies, D., Su, Z., Hazeldine, J., Lazzarino, G., Hill, L. J., Crombie, N., Foster, M., Purrello, M., Logan, A., & Belli, A. (2017). MicroRNAs as Novel Biomarkers for the Diagnosis and Prognosis of Mild and Severe Traumatic Brain Injury. *Journal of Neurotrauma*, *34*(11), 1948–1956. https://doi.org/10.1089/neu.2016.4857

Fehily, B., & Fitzgerald, M. (2017). Repeated Mild Traumatic Brain Injury. *Cell Transplantation*, *26*(7), 1131–1155. https://doi.org/10.1177/0963689717714092

Feng, Y., Li, K., Roth, E., Chao, D., Mecca, C. M., Hogan, Q. H., Pawela, C., Kwok, W.-M., Camara, A. K. S., & Pan, B. (2021). Repetitive Mild Traumatic Brain Injury in Rats Impairs Cognition, Enhances Prefrontal Cortex Neuronal Activity, and Reduces Pre-synaptic Mitochondrial Function. *Frontiers in Cellular Neuroscience*, *15*, 689334. https://doi.org/10.3389/fncel.2021.689334

Fennema, E., Rivron, N., Rouwkema, J., van Blitterswijk, C., & de Boer, J. (2013). Spheroid culture as a tool for creating 3D complex tissues. *Trends in Biotechnology*, *31*(2), 108–115. https://doi.org/10.1016/j.tibtech.2012.12.003

Fernández-Arjona, M. del M., Grondona, J. M., Granados-Durán, P., Fernández-Llebrez, P., & López-Ávalos, M. D. (2017). Microglia Morphological Categorization in a Rat Model of Neuroinflammation by Hierarchical Cluster and Principal Components Analysis. *Frontiers in Cellular Neuroscience*, *11*. https://www.frontiersin.org/article/10.3389/fncel.2017.00235

Galarraga-Vinueza, M. E., Obreja, K., Ramanauskaite, A., Magini, R., Begic, A., Sader, R., & Schwarz, F. (2021). Macrophage polarization in peri-implantitis lesions. *Clinical Oral Investigations*, *25*(4), 2335–2344. https://doi.org/10.1007/s00784-020-03556-2

Gao, J., Grill, R. J., Dunn, T. J., Bedi, S., Labastida, J. A., Hetz, R. A., Xue, H., Thonhoff, J. R., DeWitt, D. S., Prough, D. S., Cox, C. S., & Wu, P. (2016). Human Neural Stem Cell Transplantation-Mediated Alteration of Microglial/Macrophage Phenotypes after Traumatic

Brain Injury. *Cell Transplantation*, *25*(10), 1863–1877. https://doi.org/10.3727/096368916X691150

Gogola, J., Hoffmann, M., & Ptak, A. (2020). Persistent endocrine-disrupting chemicals found in human follicular fluid stimulate IGF1 secretion by adult ovarian granulosa cell tumor spheroids and thereby increase proliferation of non-cancer ovarian granulosa cells. *Toxicology in Vitro*, *65*, 104769. https://doi.org/10.1016/j.tiv.2020.104769

Gómez Morillas, A., Besson, V. C., & Lerouet, D. (2021). Microglia and Neuroinflammation: What Place for P2RY12? *International Journal of Molecular Sciences*, *22*(4), 1636. https://doi.org/10.3390/ijms22041636

Guskiewicz, K. M., Marshall, S. W., Bailes, J., McCrea, M., Cantu, R. C., Randolph, C., & Jordan, B. D. (2005). Association between Recurrent Concussion and Late-Life Cognitive Impairment in Retired Professional Football Players. *Neurosurgery*, *57*(4), 719–726. https://doi.org/10.1093/neurosurgery/57.4.719

Harvey, L. D., Yin, Y., Attarwala, I. Y., Begum, G., Deng, J., Yan, H. Q., Dixon, C. E., & Sun, D. (2015). Administration of DHA Reduces Endoplasmic Reticulum Stress-Associated Inflammation and Alters Microglial or Macrophage Activation in Traumatic Brain Injury. *ASN Neuro*, *7*(6), 1759091415618969. https://doi.org/10.1177/1759091415618969

Haynes, S. E., Hollopeter, G., Yang, G., Kurpius, D., Dailey, M. E., Gan, W.-B., & Julius, D. (2006). The P2Y12 receptor regulates microglial activation by extracellular nucleotides. *Nature Neuroscience*, *9*(12), 1512–1519. https://doi.org/10.1038/nn1805

He, J., Zhang, N., Zhu, Y., Jin, R., & Wu, F. (2021). MSC spheroids-loaded collagen hydrogels simultaneously promote neuronal differentiation and suppress inflammatory reaction through PI3K-Akt signaling pathway. *Biomaterials*, *265*, 120448. https://doi.org/10.1016/j.biomaterials.2020.120448

Heindl, S., Gesierich, B., Benakis, C., Llovera, G., Duering, M., & Liesz, A. (2018). Automated Morphological Analysis of Microglia After Stroke. *Frontiers in Cellular Neuroscience*, *12*. https://www.frontiersin.org/article/10.3389/fncel.2018.00106

Hiskens, M. I., Vella, R. K., Schneiders, A. G., & Fenning, A. S. (2021). Minocycline improves cognition and molecular measures of inflammation and neurodegeneration following repetitive mTBI. *Brain Injury*, *35*(7), 831–841. https://doi.org/10.1080/02699052.2021.1909139

Hovens, I. B., Nyakas, C., & Schoemaker, R. G. (2014). A novel method for evaluating microglial activation using ionized calcium-binding adaptor protein-1 staining: Cell body to cell size ratio. *Neuroimmunology and Neuroinflammation*, *1*, 82–88. https://doi.org/10.4103/2347-8659.139719

Humble, S. S., Wilson, L. D., Wang, L., Long, D. A., Smith, M. A., Siktberg, J. C., Mirhoseini, M. F., Bhatia, A., Pruthi, S., Day, M. A., Muehlschlegel, S., & Patel, M. B. (2018). Prognosis of Diffuse Axonal Injury with Traumatic Brain Injury. *The Journal of Trauma and Acute Care Surgery*, *85*(1), 155–159. https://doi.org/10.1097/TA.0000000000001852

IHC Troubleshooting | Abcam. (n.d.). Retrieved February 1, 2022, from https://www.abcam.com/help/troubleshooting-and-using-controls-in-ihc-and-icc

Immunohistochemistry (IHC): The complete guide | Abcam. (n.d.). Retrieved October 25, 2021, from https://www.abcam.com/content/immunohistochemistry-the-complete-guide#detection%20and%20amplification

Jassam, Y. N., Izzy, S., Whalen, M., McGavern, D. B., & Khoury, J. E. (2017). Neuroimmunology of Traumatic Brain Injury: Time for a Paradigm Shift. *Neuron*, *95*(6), 1246–1265. https://doi.org/10.1016/j.neuron.2017.07.010

Jeter, C. B., Hergenroeder, G. W., Hylin, M. J., Redell, J. B., Moore, A. N., & Dash, P. K. (2013). Biomarkers for the Diagnosis and Prognosis of Mild Traumatic Brain Injury/Concussion. *Journal of Neurotrauma*, *30*(8), 657–670. https://doi.org/10.1089/neu.2012.2439

Ji, J., Xue, T.-F., Guo, X.-D., Yang, J., Guo, R.-B., Wang, J., Huang, J.-Y., Zhao, X.-J., & Sun, X.-L. (2018). Antagonizing peroxisome proliferator-activated receptor γ facilitates M1-to-M2 shift of microglia by enhancing autophagy via the LKB1–AMPK signaling pathway. *Aging Cell*, *17*(4), e12774. https://doi.org/10.1111/acel.12774

Jiang, Q., Wei, D., He, X., Gan, C., Long, X., & Zhang, H. (2021). Phillyrin Prevents Neuroinflammation-Induced Blood–Brain Barrier Damage Following Traumatic Brain Injury via Altering Microglial Polarization. *Frontiers in Pharmacology*, *12*, 719823. https://doi.org/10.3389/fphar.2021.719823

Jin, X., Ishii, H., Bai, Z., Itokazu, T., & Yamashita, T. (2012). Temporal Changes in Cell Marker Expression and Cellular Infiltration in a Controlled Cortical Impact Model in Adult Male C57BL/6 Mice. *PLOS ONE*, *7*(7), e41892. https://doi.org/10.1371/journal.pone.0041892

Johnson, V. E., Stewart, W., & Smith, D. H. (2013). Axonal pathology in traumatic brain injury. *Experimental Neurology*, *246*, 35–43. https://doi.org/10.1016/j.expneurol.2012.01.013

Jorfi, M., D'Avanzo, C., Kim, D. Y., & Irimia, D. (2018). Three-Dimensional Models of the Human Brain Development and Diseases. *Advanced Healthcare Materials*, *7*(1), 1700723. https://doi.org/10.1002/adhm.201700723

Jurga, A. M., Paleczna, M., & Kuter, K. Z. (2020). Overview of General and Discriminating Markers of Differential Microglia Phenotypes. *Frontiers in Cellular Neuroscience*, *14*. https://www.frontiersin.org/article/10.3389/fncel.2020.00198

Karperien, A., Jelinek, H., & Milosevic, N. (2011, June 28). *Lacunarity Analysis and Classification of Microglia in Neuroscience*. https://doi.org/10.13140/2.1.3576.6082

Karve, I. P., Taylor, J. M., & Crack, P. J. (2016). The contribution of astrocytes and microglia to traumatic brain injury. *British Journal of Pharmacology*, *173*(4), 692–702. https://doi.org/10.1111/bph.13125

Kim, D. H., Kim, D. H., Heck, B. E., Shaffer, M., Yoo, K. H., & Hur, J. (2020). PPAR-δ agonist affects adipo-chondrogenic differentiation of human mesenchymal stem cells through the expression of PPAR-γ. *Regenerative Therapy*, *15*, 103–111. https://doi.org/10.1016/j.reth.2020.07.003

Koerte, I. K., Hufschmidt, J., Muehlmann, M., Lin, A. P., & Shenton, M. E. (2016). Advanced Neuroimaging of Mild Traumatic Brain Injury. In D. Laskowitz & G. Grant (Eds.), *Translational Research in Traumatic Brain Injury*. CRC Press/Taylor and Francis Group. http://www.ncbi.nlm.nih.gov/books/NBK326714/

Koizumi, S., Ohsawa, K., Inoue, K., & Kohsaka, S. (2013). Purinergic receptors in microglia: Functional modal shifts of microglia mediated by P2 and P1 receptors. *Glia*, *61*(1), 47–54. https://doi.org/10.1002/glia.22358

Kontos, A. P., Kotwal, R. S., Elbin, R. j., Lutz, R. H., Forsten, R. D., Benson, P. J., & Guskiewicz, K. M. (2013). Residual Effects of Combat-Related Mild Traumatic Brain Injury. *Journal of Neurotrauma*, *30*(8), 680–686. https://doi.org/10.1089/neu.2012.2506

Kulkarni, P., Morrison, T. R., Cai, X., Iriah, S., Simon, N., Sabrick, J., Neuroth, L., & Ferris, C. F. (2019). Neuroradiological Changes Following Single or Repetitive Mild TBI. *Frontiers in Systems Neuroscience*, *13*, 34. https://doi.org/10.3389/fnsys.2019.00034

Kumar, A., Alvarez-Croda, D.-M., Stoica, B. A., Faden, A. I., & Loane, D. J. (2016). Microglial/Macrophage Polarization Dynamics following Traumatic Brain Injury. *Journal of Neurotrauma*, *33*(19), 1732–1750. https://doi.org/10.1089/neu.2015.4268

Kumar, A., Barrett, J. P., Alvarez-Croda, D.-M., Stoica, B. A., Faden, A. I., & Loane, D. J. (2016). NOX2 drives M1-like microglial/macrophage activation and neurodegeneration following experimental traumatic brain injury. *Brain, Behavior, and Immunity*, *58*, 291–309. https://doi.org/10.1016/j.bbi.2016.07.158

Kumar, A., Stoica, B. A., Loane, D. J., Yang, M., Abulwerdi, G., Khan, N., Kumar, A., Thom, S. R., & Faden, A. I. (2017). Microglial-derived microparticles mediate neuroinflammation after traumatic brain injury. *Journal of Neuroinflammation*, *14*(1), 47. https://doi.org/10.1186/s12974-017-0819-4

Levin, H. S., & Diaz-Arrastia, R. R. (2015). Diagnosis, prognosis, and clinical management of mild traumatic brain injury. *The Lancet Neurology*, *14*(5), 506–517. https://doi.org/10.1016/S1474-4422(15)00002-2

Li, F., Cao, L., Parikh, S., & Zuo, R. (2020). Three-Dimensional Spheroids With Primary Human Liver Cells and Differential Roles of Kupffer Cells in Drug-Induced Liver Injury. *Journal of Pharmaceutical Sciences*, *109*(6), 1912–1923. https://doi.org/10.1016/j.xphs.2020.02.021

Li, Y., Zhu, Z.-Y., Lu, B.-W., Huang, T.-T., Zhang, Y.-M., Zhou, N.-Y., Xuan, W., Chen, Z.-A., Wen, D.-X., Yu, W.-F., & Li, P.-Y. (2019). Rosiglitazone ameliorates tissue plasminogen activator-induced brain hemorrhage after stroke. *CNS Neuroscience & Therapeutics*, *25*(12), 1343–1352. https://doi.org/10.1111/cns.13260

Liu, J., Abate, W., Xu, J., Corry, D., Kaul, B., & Jackson, S. K. (2011). Three-dimensional spheroid cultures of A549 and HepG2 cells exhibit different lipopolysaccharide (LPS) receptor expression and LPS-induced cytokine response compared with monolayer cultures. *Innate Immunity*, *17*(3), 245–255. https://doi.org/10.1177/1753425910365733

Lucke-Wold, B. P., Logsdon, A. F., Nguyen, L., Eltanahay, A., Turner, R. C., Bonasso, P., Knotts, C., Moeck, A., Maroon, J. C., Bailes, J. E., & Rosen, C. L. (2018). Supplements, nutrition, and alternative therapies for the treatment of traumatic brain injury. *Nutritional Neuroscience*, *21*(2), 79–91. https://doi.org/10.1080/1028415X.2016.1236174

Luo, Y., Yin, W., Signore, A. P., Zhang, F., Hong, Z., Wang, S., Graham, S. H., & Chen, J. (2006). Neuroprotection against focal ischemic brain injury by the peroxisome proliferator-activated

receptor-γ agonist rosiglitazone. *Journal of Neurochemistry*, *97*(2), 435–448. https://doi.org/10.1111/j.1471-4159.2006.03758.x

Maas, A. I., Stocchetti, N., & Bullock, R. (2008). Moderate and severe traumatic brain injury in adults. *The Lancet Neurology*, *7*(8), 728–741. https://doi.org/10.1016/S1474-4422(08)70164-9

Marklund, N. (2016). Rodent Models of Traumatic Brain Injury: Methods and Challenges. In F. H. Kobeissy, C. E. Dixon, R. L. Hayes, & S. Mondello (Eds.), *Injury Models of the Central Nervous System: Methods and Protocols* (pp. 29–46). Springer. https://doi.org/10.1007/978-1-4939-3816-2_3

McGinn, M. J., & Povlishock, J. T. (2016). Pathophysiology of Traumatic Brain Injury. *Neurosurgery Clinics of North America*, *27*(4), 397–407. https://doi.org/10.1016/j.nec.2016.06.002

McInnes, K., Friesen, C. L., MacKenzie, D. E., Westwood, D. A., & Boe, S. G. (2017). Mild Traumatic Brain Injury (mTBI) and chronic cognitive impairment: A scoping review. *PLOS ONE*, *12*(4), e0174847. https://doi.org/10.1371/journal.pone.0174847

Mckee, A. C., & Daneshvar, D. H. (2015). The neuropathology of traumatic brain injury. *Handbook of Clinical Neurology*, *127*, 45–66. https://doi.org/10.1016/B978-0-444-52892-6.00004-0

Moore, C. S., Ase, A. R., Kinsara, A., Rao, V. T. S., Michell-Robinson, M., Leong, S. Y., Butovsky, O., Ludwin, S. K., Séguéla, P., Bar-Or, A., & Antel, J. P. (2015). P2Y12 expression and function in alternatively activated human microglia. *Neurology - Neuroimmunology Neuroinflammation*, *2*(2). https://doi.org/10.1212/NXI.0000000000000080

Najem, D., Rennie, K., Ribecco-Lutkiewicz, M., Ly, D., Haukenfrers, J., Liu, Q., Nzau, M., Fraser, D. D., & Bani-Yaghoub, M. (2018). Traumatic brain injury: Classification, models, and markers. *Biochemistry and Cell Biology*. https://doi.org/10.1139/bcb-2016-0160

Nakamura, R., Nishimura, T., Ochiai, T., Nakada, S., Nagatani, M., & Ogasawara, H. (2013). Availability of a Microglia and Macrophage Marker, Iba-1, for Differential Diagnosis of

Spontaneous Malignant Reticuloses from Astrocytomas in Rats. *Journal of Toxicologic Pathology*, *26*(1), 55–60. https://doi.org/10.1293/tox.26.55

NeuN antibodies: Important tools for neuroscience | Abcam. (n.d.). Retrieved October 25, 2021, from https://www.abcam.com/neuroscience/neun-antibodies-important-tools-for-neuroscience

Ng, S. Y., & Lee, A. Y. W. (2019). Traumatic Brain Injuries: Pathophysiology and Potential Therapeutic Targets. *Frontiers in Cellular Neuroscience*, *13*, 528. https://doi.org/10.3389/fncel.2019.00528

Nzou, G., Wicks, R. T., Wicks, E. E., Seale, S. A., Sane, C. H., Chen, A., Murphy, S. V., Jackson, J. D., & Atala, A. J. (2018). Human Cortex Spheroid with a Functional Blood Brain Barrier for High-Throughput Neurotoxicity Screening and Disease Modeling. *Scientific Reports*, *8*(1), 7413. https://doi.org/10.1038/s41598-018-25603-5

Pankratova, N., Jović, M., & Pfeifer, M. E. (2021). Electrochemical sensing of blood proteins for mild traumatic brain injury (mTBI) diagnostics and prognostics: Towards a point-of-care application. *Rsc Advances*, *11*(28), 17301–17319. https://doi.org/10.1039/d1ra00589h

Peng, J., Wang, K., Xiang, W., Li, Y., Hao, Y., & Guan, Y. (2019). Rosiglitazone polarizes microglia and protects against pilocarpine-induced status epilepticus. *CNS Neuroscience & Therapeutics*, *25*(12), 1363–1372. https://doi.org/10.1111/cns.13265

Peruzzaro, S. T., Andrews, M. M. M., Al-Gharaibeh, A., Pupiec, O., Resk, M., Story, D., Maiti, P., Rossignol, J., & Dunbar, G. L. (2019). Transplantation of mesenchymal stem cells genetically engineered to overexpress interleukin-10 promotes alternative inflammatory response in rat model of traumatic brain injury. *Journal of Neuroinflammation*, *16*(1), 2. https://doi.org/10.1186/s12974-018-1383-2

Pham, L., Wright, D. K., O'Brien, W. T., Bain, J., Huang, C., Sun, M., Casillas-Espinosa, P. M., Shah, A. D., Schittenhelm, R. B., Sobey, C. G., Brady, R. D., O'Brien, T. J., Mychasiuk, R., Shultz, S. R., & McDonald, S. J. (2021). Behavioral, axonal, and proteomic alterations

following repeated mild traumatic brain injury: Novel insights using a clinically relevant rat model. *Neurobiology of Disease*, *148*, 105151. https://doi.org/10.1016/j.nbd.2020.105151

Ponomarenko, A. I., Tyrtyshnaia, A. A., Pislyagin, E. A., Dyuizen, I. V., Sultanov, R. M., & Manzhulo, I. V. (2021). N-docosahexaenoylethanolamine reduces neuroinflammation and cognitive impairment after mild traumatic brain injury in rats. *Scientific Reports*, *11*(1), 756. https://doi.org/10.1038/s41598-020-80818-9

Prince, C., & Bruhns, M. E. (2017). Evaluation and Treatment of Mild Traumatic Brain Injury: The Role of Neuropsychology. *Brain Sciences*, *7*(8), 105. https://doi.org/10.3390/brainsci7080105

Ren, L., Li, Q., Hu, X., Yang, Q., Du, M., Xing, Y., Wang, Y., Li, J., & Zhang, L. (2020). A Novel Mechanism of bta-miR-210 in Bovine Early Intramuscular Adipogenesis. *Genes*, *11*(6), 601. https://doi.org/10.3390/genes11060601

Report to Congress: Traumatic Brain Injury in the United States | Concussion | Traumatic Brain Injury | CDC Injury Center. (2019, January 31). https://www.cdc.gov/traumaticbraininjury/pubs/tbi_report_to_congress.html

Ryu, N.-E., Lee, S.-H., & Park, H. (2019). Spheroid Culture System Methods and Applications for Mesenchymal Stem Cells. *Cells*, *8*(12), 1620. https://doi.org/10.3390/cells8121620

Schmidt-Kastner, R., Wietasch, K., Weigel, H., & Eysel, U. t. (1993). Immunohistochemical staining for glial fibrillary acidic protein (GFAP) after deafferentation or ischemic infarction in rat visual system: Features of reactive and damaged astrocytes. *International Journal of Developmental Neuroscience*, *11*(2), 157–174. https://doi.org/10.1016/0736-5748(93)90076-P

Simon, D. W., McGeachy, M. J., Bayır, H., Clark, R. S. B., Loane, D. J., & Kochanek, P. M. (2017). The far-reaching scope of neuroinflammation after traumatic brain injury. *Nature Reviews Neurology*, *13*(3), 171–191. https://doi.org/10.1038/nrneurol.2017.13

Slemmer, J. E., Matser, E. J. T., De Zeeuw, C. I., & Weber, J. T. (2002). Repeated mild injury causes cumulative damage to hippocampal cells. *Brain*, *125*(12), 2699–2709. https://doi.org/10.1093/brain/awf271

Sloan, S. A., Andersen, J., Paşca, A. M., Birey, F., & Paşca, S. P. (2018). Generation and assembly of human brain region–specific three-dimensional cultures. *Nature Protocols*, *13*(9), 2062–2085. https://doi.org/10.1038/s41596-018-0032-7

Smith, D. H., Meaney, D. F., & Shull, W. H. (2003). Diffuse Axonal Injury in Head Trauma. *The Journal of Head Trauma Rehabilitation*, *18*(4), 307–316.

Taib, T., Leconte, C., Steenwinckel, J. V., Cho, A. H., Palmier, B., Torsello, E., Kuen, R. L., Onyeomah, S., Ecomard, K., Benedetto, C., Coqueran, B., Novak, A.-C., Deou, E., Plotkine, M., Gressens, P., Marchand-Leroux, C., & Besson, V. C. (2017). Neuroinflammation, myelin and behavior: Temporal patterns following mild traumatic brain injury in mice. *PLOS ONE*, *12*(9), e0184811. https://doi.org/10.1371/journal.pone.0184811

Tarnowski, B. I., Spinale, F. G., & Nicholson, J. H. (1991). DAPI as a useful stain for nuclear quantitation. *Biotechnic & Histochemistry: Official Publication of the Biological Stain Commission*, *66*(6), 297–302.

Teasdale, G., Maas, A., Lecky, F., Manley, G., Stocchetti, N., & Murray, G. (2014). The Glasgow Coma Scale at 40 years: Standing the test of time. *The Lancet Neurology*, *13*(8), 844–854. https://doi.org/10.1016/S1474-4422(14)70120-6

Toledano Furman, N. E., Prabhakara, K. S., Bedi, S., Cox Jr, C. S., & Olson, S. D. (2018). OMIP-041: Optimized multicolor immunofluorescence panel rat microglial staining protocol. *Cytometry Part A*, *93*(2), 182–185. https://doi.org/10.1002/cyto.a.23267

Toledano Furman, N., Gottlieb, A., Prabhakara, K. S., Bedi, S., Caplan, H. W., Ruppert, K. A., Srivastava, A. K., Olson, S. D., & Cox, C. S. (2020). High-resolution and differential analysis of rat microglial markers in traumatic brain injury: Conventional flow cytometric and

bioinformatics analysis. *Scientific Reports*, *10*(1), 11991. https://doi.org/10.1038/s41598-020-68770-0

Traumatic Brain Injury – Causes, Symptoms and Treatments. (n.d.). Retrieved January 23, 2022, from https://www.aans.org/

Traumatic Brain Injury Information Page | National Institute of Neurological Disorders and Stroke. (n.d.). Retrieved January 23, 2022, from https://www.ninds.nih.gov/Disorders/All-Disorders/Traumatic-Brain-Injury-Information-Page

Wang, G., Zhang, J., Hu, X., Zhang, L., Mao, L., Jiang, X., Liou, A. K.-F., Leak, R. K., Gao, Y., & Chen, J. (2013). Microglia/macrophage polarization dynamics in white matter after traumatic brain injury. *Journal of Cerebral Blood Flow & Metabolism*, *33*(12), 1864–1874. https://doi.org/10.1038/jcbfm.2013.146

Wen, L., You, W., Wang, H., Meng, Y., Feng, J., & Yang, X. (2018). Polarization of Microglia to the M2 Phenotype in a Peroxisome Proliferator-Activated Receptor Gamma–Dependent Manner Attenuates Axonal Injury Induced by Traumatic Brain Injury in Mice. *Journal of Neurotrauma*, *35*(19), 2330–2340. https://doi.org/10.1089/neu.2017.5540

WenLiang, YouWendong, WangHao, MengYuanyuan, FengJunfeng, & YangXiaofeng. (2018). Polarization of Microglia to the M2 Phenotype in a Peroxisome Proliferator-Activated Receptor Gamma–Dependent Manner Attenuates Axonal Injury Induced by Traumatic Brain Injury in Mice. *Journal of Neurotrauma*. https://doi.org/10.1089/neu.2017.5540

Witcher, K. G., Eiferman, D. S., & Godbout, J. P. (2015). Priming the Inflammatory Pump of the CNS after Traumatic Brain Injury. *Trends in Neurosciences*, *38*(10), 609–620. https://doi.org/10.1016/j.tins.2015.08.002

Wu, H., Zheng, J., Xu, S., Fang, Y., Wu, Y., Zeng, J., Shao, A., Shi, L., Lu, J., Mei, S., Wang, X., Guo, X., Wang, Y., Zhao, Z., & Zhang, J. (2021). Mer regulates microglial/macrophage M1/M2

polarization and alleviates neuroinflammation following traumatic brain injury. *Journal of Neuroinflammation*, *18*(1), 2. https://doi.org/10.1186/s12974-020-02041-7

Yang, J., Cao, L.-L., Wang, X.-P., Guo, W., Guo, R.-B., Sun, Y.-Q., Xue, T.-F., Cai, Z.-Y., Ji, J., Cheng, H., & Sun, X.-L. (2021). Neuronal extracellular vesicle derived miR-98 prevents salvageable neurons from microglial phagocytosis in acute ischemic stroke. *Cell Death & Disease*, *12*(1), 1–16. https://doi.org/10.1038/s41419-020-03310-2

Yi, J.-H., Park, S.-W., Brooks, N., Lang, B. T., & Vemuganti, R. (2008). PPARγ agonist rosiglitazone is neuroprotective after traumatic brain injury via anti-inflammatory and anti-oxidative mechanisms. *Brain Research*, *1244*, 164–172. https://doi.org/10.1016/j.brainres.2008.09.074

Yip, P. K., Hasan, S., Liu, Z.-H., & Uff, C. E. G. (2022). Characterisation of Severe Traumatic Brain Injury Severity from Fresh Cerebral Biopsy of Living Patients: An Immunohistochemical Study. *Biomedicines*, *10*(3), 518. https://doi.org/10.3390/biomedicines10030518

Younger, D., Murugan, M., Rama Rao, K. V., Wu, L.-J., & Chandra, N. (2019). Microglia Receptors in Animal Models of Traumatic Brain Injury. *Molecular Neurobiology*, *56*(7), 5202–5228. https://doi.org/10.1007/s12035-018-1428-7

Zhao, Q., Xie, F., Guo, D., Ju, F., He, J., Yao, T., Zhao, P., Pan, S., & Ma, X. (2020). Hydrogen inhalation inhibits microglia activation and neuroinflammation in a rat model of traumatic brain injury. *Brain Research*, *1748*, 147053. https://doi.org/10.1016/j.brainres.2020.147053

Zhu, M., Lin, J., Qing, P., Pu, L., Chen, S., Lin, S., Li, C., Cao, L., & Zhang, Y. (2020). Manual acupuncture relieves microglia-mediated neuroinflammation in a rat model of traumatic brain injury by inhibiting the RhoA/ROCK2 pathway. *Acupuncture in Medicine*, *38*(6), 426–434. https://doi.org/10.1177/0964528420912248